New Experimental Constraints on Clumped Isotope Bond Reordering in Dolomite

Paul Petschnig[1], Nathan Looser[1], Jordon D. Hemingway[1], Max W. Schmidt[1], Stefano M. Bernasconi[1]

[1] Department of Earth Sciences, ETH Zurich, Sonneggstrasse 5, CH-8092 Zurich, Switzerland.

Corresponding author: Stefano Bernasconi (stefano.bernasconi@erdw.ethz.ch)

Key Points:

- New dolomite clumped reordering experiments with sedimentary dolomites
- Poorly-ordered dolomite show rapid alteration of clumped isotope composition
- Dolomie-specific reordering parameters are presented

Abstract

The conditions controlling the formation of sedimentary dolomite are still poorly understood despite decades of research. Reconstructing formation temperatures and $\delta^{18}O$ of fluids from which dolomite has precipitated is fundamental to constrain dolomitization models. Carbonate clumped isotopes are a very reliable technique to acquire such information if the original composition at the time of precipitation is preserved. Sedimentary dolomite first mostly forms as a poorly-ordered metastable phase (protodolomite) and subsequently transform to the more stable ordered phase. Due to this conversion its important to determine if the original clumped isotope composition of the disordered phase is preserved during diagenetic conversion to ordered dolomite, and how resistant clumped isotope signatures are against bond reordering at elevated temperatures during burial diagenesis. Here, we present a series of heating experiments at temperatures between 360 and 480 °C with durations between 0.125 and 426 hours. We uses fine-grained sedimentary dolomites to test the influence of grains size, and cation ordering on bond reordering kinetics. We analyzed a lacustrine dolomite with poor cation ordering and well ordered a replacement dolomite, both being almost stoichiometric. The poorly ordered dolomite shows a very rapid alteration of its bulk isotope composition and higher susceptibility to solid state bond reordering, whereas the well-ordered dolomite behaves like a previously studied coarse-grained hydrothermal dolomite. We derive dolomite-specific reordering kinetic parameters for ordered dolomitea and show that Δ_{47} reordering in dolomite is material specific. Our results call for further temperature-time series experiments to constrain dolomite Δ_{47} reordering over geologic timescales.

1 Introduction

Dolomite (Ca, Mg $(CO_3)_2$) is a widespread mineral in the sedimentary rock record but its very rare in Holocene sediments (see Manche & Kaczmarek (2021) for a recent review). The low abundance of dolomite in modern marine sediments, although modern seawater is supersaturated with respect to dolomite and the difficulty to precipitate dolomite at low temperatures is the key of the dolomite problem (see e.g. (Arvidson & Mackenzie, 1999). Dolomite can form as a replacement of calcitic or aragonitic sediments or as a direct precipitation from a solution as a fine-grained mud or as a cement in cavities and fractures (e.g. (Machel, 2004). Most dolomites in the geologic record formed via the diagenetic replacement of limestone during reaction with Mg-bearing fluids derived from sea water, ground and/or lacustrine waters, or basinal brines (Machel, 2004).

Most laboratory studies aimed at precipitating dolomite at ambient temperatures have only produced poorly ordered dolomites (proto-dolomites), which lack the crystallographic ordering of most ancient natural dolomites (Gregg et al., 2015; Manche & Kaczmarek, 2021; Pina et al., 2020). It has to be noted, though that also in the geological record the variability in stoichiometry and cation ordering in considerable in the entire phanerozoic (Manche & Kaczmarek, 2021). Besides temperature, several parameters such as rock porosity, fluid composition, and water/rock ratios influence the formation of dolomite (Gregg et al., 2015; Warren, 2000.. In modern near-surface environments, (proto)dolomite formation is thought to be promoted by microbial activity (Brauchli et al., 2016; Vasconcelos & McKenzie, 1997; Wright & Wacey, 2005).

The study of naturally occurring, multiply substituted isotopologues, or “clumped isotopes”, in recent years has developed into a broad field with several applications. This has led

to a wide range of palaeothermometry studies, including paleo-climate reconstruction (Came et al., 2007; Vickers et al., 2020, 2021), diagenetic and metamorphic processes (Brenner et al., 2021; Lloyd et al., 2017; Millán et al., 2016), and burial-history reconstruction of sedimentary basins and tectonics (Looser et al., 2021). Compared to classical oxygen isotope geothermometry, which requires knowledge of the oxygen isotope composition of the fluid to calculate formation temperatures, clumped isotope thermometry is independent of the fluid composition from which the carbonate precipitated (Ghosh et al., 2006; Schauble et al., 2006). Another key advantage of clumped isotope thermometry is the possibility to calculate the $\delta^{18}O$ of fluid in equilibrium with carbonate (Eiler, 2011; Ghosh et al., 2006), giving further insights into the conditions under which carbonate minerals were formed.

A major potential limitation of carbonate clumped isotope thermometry is the modification of original clumped isotope signatures by heating during burial diagenesis and/or metamorphic events, which can significantly alter the original Δ_{47} values. This alteration may occur without mineralogical alteration through so called "solid state bond reordering." Ghosh et al. (2006) observed unrealistically low Δ_{47}-derived temperatures of ~200 °C for a calcite marble and proposed that a closed system solid-state isotope exchange among the carbonate ions is responsible for altering the original clumped isotope abundance in carbonates upon cooling. Schmid & Bernasconi (2010)) and Dennis & Schrag (2010) similarly measured carbonate minerals in carbonatites and marbles and found that samples with a true crystallization temperature of >500 °C record a Δ_{47}-derived temperatures of ~100 to 300 °C. Nevertheless, it remained unclear whether these temperatures actually reflect the kinetics of intra-crystalline isotope effects or whether, at least in some of the samples which showed also anomalous carbon and oxygen isotope compositions, they result from recrystallization. (Passey & Henkes, 2012) and Henkes et al. (2014) laid the foundation for the quantitative interpretation of isotope bond reordering in carbonates by performing and modeling heating experiments on optical, sparry, and brachiopod calcites to determine the extent and the kinetics of isotope reordering upon progressive heating. These experiments directly demonstrated that solid-state bond reordering alone can explain observed apparent equilibrium blocking temperatures in nature, with no open system isotope exchange and/or recrystallization.

In general, diffusional solid-state bond reordering occurs via exchange of carbon and oxygen atoms between neighboring carbonate groups within the crystal lattice. For C and O to diffuse, C-O bonds must be broken and reformed, a process strongly dependent on temperature and the time of exposure to elevated temperatures. For example, the temperature range 80-120 °C is thought to be the critical temperature at which calcite solid-state bond reordering initiates and leads to measurable Δ_{47} changes over geological timescales (Henkes et al., 2014; Passey & Henkes, 2012; Stolper & Eiler, 2015). Importantly, and in contrast to recrystallization, intra-crystalline diffusion does not alter petrological, textural, elemental and bulk isotope characteristics. In other words, a carbonate undergoing solid-state bond reordering only changes its Δ_{47} composition but remains unchanged in all other aspects (Henkes et al., 2014; Shenton et al., 2015; Stolper & Eiler, 2015), making this process difficult to detect and quantify in nature.

Mineralogy appears to be the most important controlling factor on reordering rates. Of all previously investigated minerals (i.e., calcite, aragonite, dolomite, and the carbonate group in apatite), aragonite exhibits the fastest and dolomite the slowest reordering rates (Chen et al., 2019; Lloyd et al., 2017, 2018; Ryb et al., 2017; Stolper & Eiler, 2015). Still, although several studies have calibrated the dolomite clumped isotope thermometer (Anderson et al., 2021;

Bonifacie et al., 2017; Müller et al., 2019; Winkelstern et al., 2016), to date the only experimental study of dolomite solid-state bond reordering rates comes from (Lloyd et al., 2018), who analyzed an optical-grade, high temperature hydrothermal dolomite from Eugui, Spain. This dolomite is stoichiometric and well ordered; it precipitated as rhombohedral crystals from a hydrothermal fluid at 160 to 170 °C (Lugli et al., 2000; Martinez et al., 1996; Reeder & Wenk, 1983). The heating-experiment with Eugui dolomite suggest that dolomite Δ_{47} values are resistant to bond reordering at diagenetic temperatures up to 150 °C over geologic timescales (Lloyd et al., 2018). However, dolomite in the geologic record differs greatly in ordering ratio, stoichiometry, and crystallinity (Manche & Kaczmarek, 2021). Furthermore, other factors such as pressure, internal water content, and trace or minor element substitutions may also influence bond reordering (Brenner et al., 2018; Chen et al., 2019; Henkes et al., 2014; Looser et al., 2023; Nooitgedacht et al., 2021; Passey & Henkes, 2012). Thus, questions remain if this resistance is uniform for all dolomite types or if mineralogical parameters impact apparent equilibrium blocking temperatures and reordering resistance.

1.2. Reordering models and the need for material-specific parameters

By performing heating experiments at several temperatures with known carbonate compositions and heating durations, one can observe Δ_{47} evolution and possible changes in mineralogy and isotope composition of reactant carbonates. Under the assumption of first-order kinetics and an Arrhenian temperature dependence, the activation energy for C-O reordering, E, and the Arrhenius pre-exponential factor, k_0, can be determined. With these parameters, Δ_{47} bond reordering can then be reconstructed for any given time-temperature (t-T) history of a specific carbonate (Hemingway & Henkes, 2021; Passey & Henkes, 2012; Stolper & Eiler, 2015).

However, there is a rapid change in Δ_{47} during the first minutes of heating observed in all existing published experiments, that clearly deviate from an exponential decrease as predicted by first-order kinetics (Henkes et al., 2014; Lloyd et al., 2018; Passey & Henkes, 2012; Stolper & Eiler, 2015). To explain this observation, three models for clumped isotope bond reordering have been developed: (i) The "transient defect/equilibrium defect" model of (Henkes et al., 2014) (hereafter "He14"), which describes non-first order behavior as a result of simultaneous reaction of two defect populations, one that follows first-order kinetics and a second where defect concentration decreases with prolonged heating due to annealing. (ii) The "paired reaction-diffusion" model of (Stolper & Eiler, 2015) (hereafter "SE15"), where the rapid initial Δ_{47} change is treated as the interaction of neighboring pairs of singly substituted carbonate groups, whereas long-term change is treated as diffusion through the crystal lattice following first-order kinetics. (iii) The "disordered kinetic" model of (Hemingway & Henkes, 2021) (hereafter "HH21"), who characterize the early, rapid change in Δ_{47} as a natural consequence of "random-walk" isotope diffusion through the mineral lattice. In this formulation, each random-walk step can be described by a unique E value that depends on the distance to neighboring atoms. The HH21 model argues for a log-normal E distribution and demonstrates that the He14 and SE15 models represent specific cases of disordered kinetics.

In addition to Δ_{47}, experiments can be used to monitor the impact of heating on bulk stable isotope values (δ^{13}C and δ^{18}O). Previous aragonite, calcite, and dolomite studies all observed constant δ^{13}C and δ^{18}O values throughout all experiments (Chen et al., 2019; Looser et al., 2023; Passey & Henkes, 2012; Stolper & Eiler, 2015). Although most experimental heating

studies make use of a CO_2 atmosphere to track potential isotope exchange, the utility of this approach is limited when experiments utilize large single crystals (i.e., mm size), since low surface area-to-volume (S/V) ratios render surficial dissolution-precipitation processes negligible in the overall isotope signal. Furthermore, the cm- to dm-sized crystals of the Eugui dolomite used by Lloyd et al. (2018), are a not the common form of dolomite in the geological record. Rather, the majority of dolomite in the sedimentary record is present as fine-grained massive dolostone which forms as a replacement of a precursor calcitic or aragonitic sediments or as primary precipitate in evaporitic environments. Sedimentary dolomites are most commonly neither perfectly stoichiometric nor perfectly ordered (Manche & Kaczmarek, 2021). As already mentioned by Lloyd et al. (2018), reordering rates may be material specific, thus necessitating kinetic results for dolomite types that are more common in nature than the optical grade, high-temperature hydrothermal Eugui dolomite.

Here, we intentionally analyze homogenous, fine-grained samples, which represent the most abundant natural dolomites, to test whether the rate constants of Δ_{47} bond reordering for distinct dolomites differ and to determine the mechanisms that drive stable- and clumped-isotope exchange. Specifically, we experimentally investigate clumped isotope reordering rates on two sedimentary low temperature dolomites: (i) a lacustrine dolomite of Pliocene age from the La Roda formation in Spain, and (ii) a replacement dolomite from the middle Triassic San Salvatore formation in Ticino, Switzerland (both previously described in Müller et al., 2017, 2019). These dolomites share a near perfect stoichiometry but differ in crystallinity and cation ordering. Comparing these two materials in identical, well-controlled experiments thus provides crucial constraints on Δ_{47} reordering and points towards material specific dolomite kinetic parameters, similar to previous observations for calcite (Looser et al., 2023).

Several experimental studies investigated this reordering for different calcite types (Brenner et al., 2018; Henkes et al., 2014; Passey & Henkes, 2012; Stolper & Eiler, 2015), but only one previous study did so for dolomite (Lloyd et al., 2018). A second important consideration for dolomite is the observation that early diagenetic sedimentary dolomites are poorly ordered, and often also non-stoichiometric, and their crystallographic ordering increases with time (Manche & Kaczmarek, 2021) potentially altering the original clumped isotope composition.

With this study, we aimed to increase the experimental database on clumped isotope solid-state bond reordering for dolomite. Specifically, we tested different dolomite materials with heating experiments to refine and improve the applicability of bond reordering kinetic models in dolomite for geological applications. Furthermore, we are the first to report all dolomite reordering results in the I-CDES reference frame (Bernasconi et al., 2021), which utilizes consistent, carbonate-based standardization; results generated here are thus directly comparable across laboratories.

1.2. Reordering models and the need for material-specific parameters

By performing heating experiments at several temperatures with known carbonate compositions and heating durations, one can observe Δ_{47} evolution and possible changes in mineralogy and isotope composition of reactant carbonates. Under the assumption of first-order kinetics and an Arrhenian temperature dependence, the activation energy for C-O reordering, E, and the Arrhenius pre-exponential factor, k_0, can be determined. With these parameters, Δ_{47} bond

reordering can then be reconstructed for any given time-temperature (t-T) history of a specific carbonate (Hemingway & Henkes, 2021; Passey & Henkes, 2012; Stolper & Eiler, 2015). However, there is a rapid change in Δ_{47} during the first minutes of heating observed in all existing published experiments, that clearly deviate from an exponential decrease as predicted by first-order kinetics (Henkes et al., 2014; Lloyd et al., 2018; Passey & Henkes, 2012; Stolper & Eiler, 2015). To explain this observation, three models for clumped isotope bond reordering have been developed: (i) The "transient defect/equilibrium defect" model of (Henkes et al., 2014) (hereafter "He14"), which describes non-first order behavior as a result of simultaneous reaction of two defect populations, one that follows first-order kinetics and a second where defect concentration decreases with prolonged heating due to annealing. (ii) The "paired reaction-diffusion" model of (Stolper & Eiler, 2015) (hereafter "SE15"), where the rapid initial Δ_{47} change is treated as the interaction of neighboring pairs of singly substituted carbonate groups, whereas long-term change is treated as diffusion through the crystal lattice following first-order kinetics. (iii) The "disordered kinetic" model of (Hemingway & Henkes, 2021) (hereafter "HH21"), who characterize the early, rapid change in Δ_{47} as a natural consequence of "random-walk" isotope diffusion through the mineral lattice. In this formulation, each random-walk step can be described by a unique *E* value that depends on the distance to neighboring atoms. The HH21 model argues for a log-normal *E* distribution and demonstrates that the He14 and SE15 models represent specific cases of disordered kinetics.

In addition to Δ_{47}, experiments can be used to monitor the impact of heating on bulk stable isotope values ($\delta^{13}C$ and $\delta^{18}O$). Previous aragonite, calcite, and dolomite studies all observed constant $\delta^{13}C$ and $\delta^{18}O$ values throughout all experiments (Chen et al., 2019; Looser et al., 2023; Passey & Henkes, 2012; Stolper & Eiler, 2015). Although most experimental heating studies make use of a CO_2 atmosphere to track potential isotope exchange, the utility of this approach is limited when experiments utilize large single crystals (i.e., mm size), since low surface area-to-volume (S/V) ratios render surficial dissolution-precipitation processes negligible in the overall isotope signal. Furthermore, the cm- to dm-sized crystals of the Eugui dolomite used by Lloyd et al. (2018), are a not the common form of dolomite in the geological record. Rather, the majority of dolomite in the sedimentary record is present as fine-grained massive dolostone which forms as a replacement of a precursor calcitic or aragonitic sediments or as primary precipitate in evaporitic environments. Sedimentary dolomites are most commonly neither perfectly stoichiometric nor perfectly ordered (Manche & Kaczmarek, 2021). As already mentioned by Lloyd et al. (2018), reordering rates may be material specific, thus necessitating kinetic results for dolomite types that are more common in nature than the optical grade, high-temperature hydrothermal Eugui dolomite.

Here, we intentionally analyze homogenous, fine-grained samples, which represent the most abundant natural dolomites, to test whether the rate constants of Δ_{47} bond reordering for distinct dolomites differ and to determine the mechanisms that drive stable- and clumped-isotope exchange. Specifically, we experimentally investigate clumped isotope reordering rates on two sedimentary low temperature dolomites: (i) a lacustrine dolomite of Pliocene age from the La Roda formation in Spain, and (ii) a replacement dolomite from the middle Triassic San Salvatore formation in Ticino, Switzerland (both previously described in Müller et al., 2017, 2019). These dolomites share a near perfect stoichiometry but differ in crystallinity and cation ordering. Comparing these two materials in identical, well-controlled experiments thus provides crucial

constraints on Δ_{47} reordering and points towards material specific dolomite kinetic parameters, similar to previous observations for calcite (Looser et al., 2023).

Several experimental studies investigated this reordering for different calcite types (Brenner et al., 2018; Henkes et al., 2014; Passey & Henkes, 2012; Stolper & Eiler, 2015), but only one previous study did so for dolomite (Lloyd et al., 2018). A second important consideration for dolomite is the observation that early diagenetic sedimentary dolomites are poorly ordered, and often also non-stoichiometric, and their crystallographic ordering increases with time (Manche & Kaczmarek, 2021) potentially altering the original clumped isotope composition.

With this study, we aimed to increase the experimental database on clumped isotope solid-state bond reordering for dolomite. Specifically, we tested different dolomite materials with heating experiments to refine and improve the applicability of bond reordering kinetic models in dolomite for geological applications. Furthermore, we are the first to report all dolomite reordering results in the I-CDES reference frame (Bernasconi et al., 2021), which utilizes consistent, carbonate-based standardization; results generated here are thus directly comparable across laboratories.

2. Materials and methods

2.1. Samples

La Roda dolomite (Rodolo) is a Pliocene lacustrine dolomite from La Roda, Spain (Garcia Del Cura et al., 2001. Our hand specimen is semi consolidated and friable; Rodolo is a very fine grained, loosely packed crystal aggregate with single crystals of ~1-5 µm size (Figure 1). Based on X-ray diffraction (XRD), it has a near perfect stoichiometry with a poor cation ordering deduced from a (015)/(110) intensity ratio of 0.31. Rodolo is described by $\Delta47 = 0.632 \pm 0.012$ ‰ (I-CDES, 95% CL), corresponding to a $\Delta47$ formation temperature of 13 ± 4 °C when using the (Anderson et al., 2021) calibration. A high initial $\Delta47$ value makes this dolomite ideal for clumped reordering studies since it is very far from theoretical $\Delta47$ equilibrium at our experimental temperatures.

Monte San Salvatore (Sansa) dolomite was taken from a road outcrop at Forca di San Martino in Ticino, Switzerland (45°58’57N; 8°57’18E). It is a compact rock containing crystalline replacement dolomite from the middle Triassic. After milling in an orbital mill, grains analyzed here are 10 – 120 µm with smaller crystals (< 2µm) attached to the crystal surfaces (Figure 1). These smaller particles are visible in unheated powder as well as in post-experimental products. We monitored these particles to track possible recrystallization at elevated temperature, since smaller crystals are expected to react faster. Like Rodolo, Sansa is described by a near perfect stoichiometry; however, unlike Rodolo, it displays a high ratio of the ordering peaks (015)/(110) of 1.03. Sansa is described by $\Delta47 = 0.505 \pm 0.013$ ‰, corresponding to a formation temperature of 61 ± 6 °C (Anderson et al., 2021b).

Both dolomites were originally described in (Müller et al., 2017) for calibration purposes. Values in Müller et al. (2019) are given in CDES 70°C (Rodolo: $\Delta47 = 0.632 \pm 0.006$ ‰; Sansa: $\Delta_{47} = 0.526 \pm 0.014$ ‰); we thus remeasured the starting materials to work consistently within the I-CDES scale (Bernasconi et al., 2021). When compared to Müller et al. (2017, 2019), our $\Delta47$ Rodolo results are statistically identical whereas Sansa $\Delta47$ values are 0.020 ‰ higher; stable isotope compositions between studies are identical within uncertainty.

2.2. Experimental setup and sample preparation

Experimental treatments for both dolomites were identical. Aliquots of ~0.178 mg of sample material and 0.046 mg of silver oxalate ($Ag_2C_2O_4$) were loaded in fused quartz glass tubes of ~8cm length and inner diameter of 7 mm. The tubes were pre-annealed at 950 °C for ~12 hours to reduce contaminations. Silver oxalate was placed between two layers of quartz wool to prevent direct contact (and possible reaction) with the sample material. Each tube was than evacuated to 6.8x10-3 bar and welded shut (supporting material, Figure S1). Silver oxalate was added for several reasons: (i) Sulphur compounds are bound by Ag to form silver sulfide (Ag_2S), thus reducing m/z 48 isobaric interferences in the mass spectrometer (see section 2.3). (ii) Its decomposition produces a slight overpressure of CO_2 in the evacuated vial, which stabilizes dolomite and hinders the reaction $Ca,Mg(CO_3)_2 \rightarrow CaCO_3 + MgO + CO_2$. An extension of the experimental series to higher temperatures using this setup was not possible since the stability of dolomite could not be ensured beyond 480 °C at ~1-2 bar pCO2 (Graf & Goldsmith, 1955). (iii) Due to the known isotopic composition of oxalate ($\delta^{13}C$ = -7.69 ‰ VPDB; $\delta^{18}O$ = +1.20 ‰ VPDB), carbon and oxygen isotope exchange between dolomite and CO2 can be tracked and potential open system recrystallization can be monitored.

All materials (quartz wool, silver oxalate, dolomite and silica vial) are dried prior to heating, and experiments started in vacuum, avoiding H_2O as much as possible. However, in spite of intensive drying, silver oxalate retains ~2 wt% H_2O (Jendrzejewski et al., 1997), which may interact with the dolomite. Possible implications of this matter are discussed in section 4.2.

Experiments were conducted in a standard box furnace using a secondary K-type thermocouple directly adjacent to the sample to account for the offset between the built-in controlling thermocouple and true sample temperature. Temperature is accurate to ± 2 °C for temperatures of 360 °C to 480 °C. Experiments were quenched by dropping the silica vials into a water bath, thus cooling samples to room temperature within seconds. After quenching, vials were reweighted, and each opened vial was cleaned with ethanol to prevent sample contamination during extraction. Vials with a significant difference to the starting weight and those with visual contact between silver oxalate and dolomite were discarded and repeated.

In total, fifty heating experiments were performed on Rodolo and Sansa dolomites at 360 °C, 420 °C and 480 °C for times ranging from 7.5 minutes to 426 hours (Table 1). To ensure identical conditions, experiments were executed in parallel with both dolomites.

2.3. Mineralogical analyses

Dolomite elemental compositions were determined by X-ray fluorescence (XRF). Unheated raw material was dried overnight at 110 °C and loss of ignition (LOI; assumed to correspond to CO_2) was determined by heating for two hours at 1050 °C. Residual material was homogenized in a 1:8 ratio with $Li_2B_4O_7$ and fused into glass beads using with a PANalytical Eagon2 automated fluxer. Glass beads were measured on a PANalytical Axios XRF spectrometer with 24-60 kV acceleration voltage and 40-100 mA current. Standardization was carried out against 35 internationally accepted standard materials.

Dolomite cell parameters were determined using powder X-ray diffraction (XRD). Approximately 20 mg of sample material was ground in an agate mortar, spread on a polished silica wafer and analyzed using a Bruker AXS D8 Advance with a Lynxeye detector, 20 KeV beam, 20-90 2-theta scan range, and a 0.02 step size with 1.5 s integration time. Dolomite stoichiometry was determined based on the position of the (104) main peak following the recipe of (Lumsden and Chimahusky, 1980). Similarly, cation ordering was monitored using the (015)/(110) ratio method from Goldsmith and Graf (1958); dolomite stoichiometry determination performed here is semi-quantitative and subject to uncertainty (see section 3.1.; (Gregg et al., 2015). Finally, to track possible recrystallization, a JEOL JSM-6390 scanning electron microscope (SEM) was used to acquire backscatter images gold coated aliquots (Figure 1).

2.4. Clumped and stable isotope analysis

Stable- and clumped-isotope analyses were conducted using a ThermoScientific Kiel IV carbonate device coupled with a ThermoScientific MAT 253 and MAT253+ isotope ratio mass spectrometer (IRMS) at the Geological Institute at ETH Zürich. Detailed method descriptions are given in (Meckler et al., 2014; Müller et al., 2017). In summary, 120-140 µg of each calcite standard or dolomite sample material were loaded into glass vials. In the Kiel IV device, three drops of 104% phosphoric acid reacts with calcite standards for 300s and with dolomite samples for 2000s at 70 °C; resulting CO_2 (and contaminant gases) is then cryogenically trapped. After the reaction is complete, gas is transferred through a Porapak Q column trap kept at -40 °C to isolate CO_2 and remove contaminant gases. At the beginning of each session, m/z 44-47 backgrounds were determined by high-voltage peak scans at five different intensities between 10 and 30 V (Bernasconi et al. 2013). All measurements were run in long integration dual inlet mode (LIDI; (Hu et al., 2014), where sample and working gas are sequentially measured for 400s. During each measurement, intensities on *m/z* 44 decrease from ~20-22 V to ~10-12 V.

In total, we analyzed 52 samples over 571 acquisitions, of which 68 were removed as outliers (11.9%). Details on outlier screening can be found in the *supporting material*. Clumped isotope data in this study are reported in the I-CDES scale (Bernasconi et al., 2021), with Δ_{47} uncertainties as 95 % confidence intervals (CI; (Fernandez et al., 2017). Equilibrium compositions and Δ_{47} temperatures are calculated using the (Anderson et al., 2021) calibration. Carbon and oxygen stable isotope compositions are given in conventional delta notation relative to Vienna Pee Dee Belemnite (VPDB) (Coplen, 2011). Data corrections and calculations were done with the Easotope software package (John & Bowen, 2016).

3. Results

3.1 Dolomite mineralogy

The crystal structure of dolomite deviates from calcite in that alternating layers of Mg^{2+} and Ca^{2+} are interspersed with CO_3^{2-} groups (Lippmann, 1973; Steinfink & Sans, 1959). A comprehensive comparison of dolomite, proto dolomite, calcite, and high-magnesium calcite can be found in (Gregg et al., 2015). Both unheated samples show the main dolomite reflections at (104), (110), and (113) and the dolomite ordering reflections at (101), (015), and (021) at the corresponding 2θ space (Goldsmith & Graf, 1958; Gregg et al., 2015). Rodolo is described by an XRF-derived Ca:Mg ratio of 51.9:48.1 ± 0.2 (1σ) whereas Sansa displays a ratio of Ca:Mg =

50.6:49.4 ± 0.2 (1σ). The ratios from XRF measurements are consistent with Mg contents estimated from dolomite reflection at the d(104) position (Lumsden, 1979; Lumsden & Chimahusky, 1980), which are Mg = 48.2 ± 0.9% and Mg = 50.0 ± 0.3% for Rodolo and Sansa, respectively (1σ, Table 1). Both samples contain minor Al_2O_3, Fe_2O_3, and SiO_2 contamination (Table S1, *supporting Information*). Elevated Al_2O_3 and SiO_2—especially in Rodolo—might result from minor clay minerals that are not detected by XRD.

We determined XRD patterns for unheated materials as well as the shortest and longest runtimes of each temperature series. At 360 °C, only the 1h hour experiment was determined since there is no significant change in isotopic composition thereafter (Table 1, Figure 3). Unheated Rodolo starting material has an ordering ratio of (015)/(110) = 0.31 ± 0.03. Within error of the technique (± 0.03 1σ), we do not see any significant changes in cation ordering during heating: at 360 and 420 °C, the ratio is (015)/(110) = 0.30 and at 480 °C after 96h heating the ordering ratio shifts slightly towards better cation ordering, with (015)/(110) = 0.36, although this is not statistically significant (± 0.03 1σ). The main dolomite ordering reflections are clearly detected in every experiment. We observe small stoichiometry variation between individual experiments, which range from 47.5-50.0% Mg (Table 1); however, we attribute this difference to sample preparation and XRD measurement uncertainty because all spectra are standardized to the quartz peak at 26.7 °2θ. A minor calcite contamination ((104) calcite, Figure 2), shown by the major 104 calcite peak, is visible throughout all experiments but does not increase upon heating.

Table 1: Results of all heating experiments. Uncertainties on $\delta^{13}C$ and $\delta^{18}O$ are reported as 1σ standard deviations, whereas Δ_{47} undertainties are reported as 95% confidence intervals. 1σ uncertainties on ordering ratios are ±0.03 and ±0.05 for Rodolo and Sansa respectively. %Mg uncertainty is ±0.9% for Rodolo and ±0.3% for Sansa.

390

Identifier	T (°C)	Time (h)	$\delta^{13}C$ (‰, VPDB)	$\delta^{18}O$ (‰, VPDB)	Δ_{47} (‰, I-CDES)	#	oredering ratio	% Mg
LaRo unheated	0	0	-3.73 ± 0.02	2.78 ± 0.08	0.632 ± 0.012	13	0.31	48.2
Rodolo 270	360	1	-3.82 ± 0.03	2.59 ± 0.07	0.551 ± 0.015	12	0.30	49.4
Rodolo 199	360	2	-3.79 ± 0.02	2.60 ± 0.08	0.585 ± 0.017	10		
Rodolo 198	360	4	-3.82 ± 0.02	2.60 ± 0.15	0.560 ± 0.019	9		
Rodolo 196	360	12	-3.81 ± 0.04	2.64 ± 0.13	0.561 ± 0.015	12		
Rodolo 160	360	96	-3.84 ± 0.02	2.62 ± 0.20	0.515 ± 0.012	12		
Rodolo 161	360	168	-3.84 ± 0.02	2.65 ± 0.14	0.513 ± 0.014	10		
Rodolo 274	420	1	-3.85 ± 0.02	2.55 ± 0.11	0.518 ± 0.019	10	0.30	49.4
Rodolo 273	420	2	-3.84 ± 0.02	2.55 ± 0.09	0.513 ± 0.025	10		
Rodolo 250	420	4	-3.84 ± 0.02	2.58 ± 0.07	0.510 ± 0.012	9		
Rodolo 251	420	8	-3.85 ± 0.02	2.55 ± 0.09	0.529 ± 0.016	10		
Rodolo 12	420	12	-3.84 ± 0.02	2.56 ± 0.11	0.537 ± 0.024	9		
Rodolo 272	420	24	-3.86 ± 0.03	2.55 ± 0.12	0.497 ± 0.023	10		
Rodolo 149	421	48	-3.83 ± 0.03	2.46 ± 0.11	0.528 ± 0.015	16		
Rodolo 150	421	96	-3.86 ± 0.02	2.39 ± 0.03	0.488 ± 0.009	11		
Rodolo 151	421	192	-3.83 ± 0.02	2.36 ± 0.06	0.518 ± 0.019	9		
Rodolo 152	421	426	-3.89 ± 0.04	2.38 ± 0.05	0.494 ± 0.015	9	0.30	49.4
Rodolo 282	480	0.125	-3.86 ± 0.03	2.46 ± 0.14	0.523 ± 0.014	13	0.29	50.0
Rodolo 283	480	0.25	-3.87 ± 0.05	2.43 ± 0.17	0.526 ± 0.019	11		
Rodolo 233	480	0.5	-3.81 ± 0.02	2.62 ± 0.10	0.532 ± 0.022	11		
Rodolo 280	480	1	-3.86 ± 0.03	2.49 ± 0.09	0.533 ± 0.011	10		
Rodolo 281	480	2	-3.87 ± 0.04	2.54 ± 0.16	0.496 ± 0.014	11		
Rodolo 232	480	4.5	-3.85 ± 0.02	2.56 ± 0.03	0.501 ± 0.023	8		
Rodolo 231	480	8	-3.85 ± 0.02	2.54 ± 0.04	0.503 ± 0.018	10		
Rodolo 176	480	24	-3.85 ± 0.01	2.44 ± 0.08	0.496 ± 0.017	11		
Rodolo 172	480	96	-4.02 ± 0.01	1.92 ± 0.05	0.454 ± 0.018	11	0.36	47.5
Sansa unheated	0	0	1.48 ± 0.04	-3.38 ± 0.12	0.505 ± 0.013	11	1.03	50.0
Sansa 271	360	1	1.45 ± 0.02	-3.46 ± 0.10	0.501 ± 0.012	10	0.95	50.0
Sansa 212	360	2	1.46 ± 0.03	-3.38 ± 0.11	0.475 ± 0.018	11		
Sansa 213	360	4	1.48 ± 0.02	-3.37 ± 0.07	0.491 ± 0.018	11		
Sansa 211	360	12	1.47 ± 0.02	-3.37 ± 0.10	0.488 ± 0.013	10		
Sansa 162	360	96	1.42 ± 0.02	-3.37 ± 0.16	0.493 ± 0.018	10		
Sansa 163	360	168	1.41 ± 0.02	-3.39 ± 0.16	0.485 ± 0.012	10		
Sansa 278	420	1	1.41 ± 0.03	-3.44 ± 0.11	0.466 ± 0.019	11	0.97	50.3
Sansa 277	420	2	1.42 ± 0.04	-3.45 ± 0.13	0.476 ± 0.016	11		
Sansa 252	420	4	1.43 ± 0.02	-3.43 ± 0.09	0.461 ± 0.013	11		
Sansa 253	420	8	1.38 ± 0.03	-3.48 ± 0.13	0.452 ± 0.017	11		
Sansa 210	420	12	1.43 ± 0.01	-3.37 ± 0.06	0.471 ± 0.015	9		
Sansa 275	420	24	1.34 ± 0.05	-3.57 ± 0.15	0.436 ± 0.015	11	0.94	49.4
Sansa 145	421	48	1.38 ± 0.03	-3.64 ± 0.07	0.425 ± 0.014	16		
Sansa 146	421	96	1.33 ± 0.04	-3.65 ± 0.10	0.434 ± 0.013	14		
Sansa 147	421	192	1.27 ± 0.02	-3.71 ± 0.10	0.405 ± 0.012	9		
Sansa 148	421	426	1.25 ± 0.05	-3.73 ± 0.10	0.420 ± 0.016	10	1.00	50.0
Sansa 285	480	0.125	1.42 ± 0.02	-3.48 ± 0.08	0.489 ± 0.009	9	1.09	49.7
Sansa 286	480	0.25	1.41 ± 0.04	-3.51 ± 0.15	0.468 ± 0.010	10		
Sansa 230	480	0.5	1.42 ± 0.02	-3.39 ± 0.07	0.455 ± 0.012	14		
Sansa 279	480	1	1.40 ± 0.03	-3.47 ± 0.12	0.443 ± 0.013	10		
Sansa 284	480	2	1.38 ± 0.04	-3.53 ± 0.12	0.444 ± 0.015	11		
Sansa 228	480	4.5	1.38 ± 0.03	-3.41 ± 0.09	0.435 ± 0.010	16		
Sansa 229	480	8	1.32 ± 0.02	-3.45 ± 0.07	0.435 ± 0.011	15		
Sansa 177	480	24	1.21 ± 0.02	-3.64 ± 0.08	0.420 ± 0.019	11		
Sansa 174	480	96	1.29 ± 0.02	-3.52 ± 0.07	0.404 ± 0.015	12	1.00	49.7

391

392

San Salvatore dolomite displays all ordering reflections for in experiments. High crystallinity in this sample leads to a dolomite (104) reflection almost two orders of magnitude larger than the other main dolomite reflections (110) and (113). Sansa starting material has a near perfect ordering ratio with (015)/(110) = 1.03 ± 0.05. After heating, ordering varies slightly between (015)/(110) = 0.94 ± 0.05 (420 °C, 24h) and (015)/(110) = 1.09 ± 0.05 (480°C, 0.125h; uncertainty is ±1σ for all acquired Sansa measurements). Because there is no obvious trend visible, this fluctuation can be attributed to sample preparation. Stoichiometry lies constantly between Mg = 49.4 ± 0.3 to 50.3 ± 0.3 % (±1σ). Like in Rodolo, a minor contamination of calcite at the (104) calcite position is visible in all patterns. Since we do not see a quartz peak in Sansa XRD, it was standardized against a stoichiometric, well ordered standard dolomite in the PDF XRD database Nr. 01-075-3697 (Antao et al., 2004). Throughout the experimental series of both samples, there is no obvious indication for recrystallization visible by XRD.

In summary, no significant changes in dolomite mineralogy are observed during heating, which underlies that dolomite does not decompose or recrystallize. Since this study's main objective is clumped isotope reordering, the results in section 3.1. give confidence in the stability of dolomite throughout the experimental range.

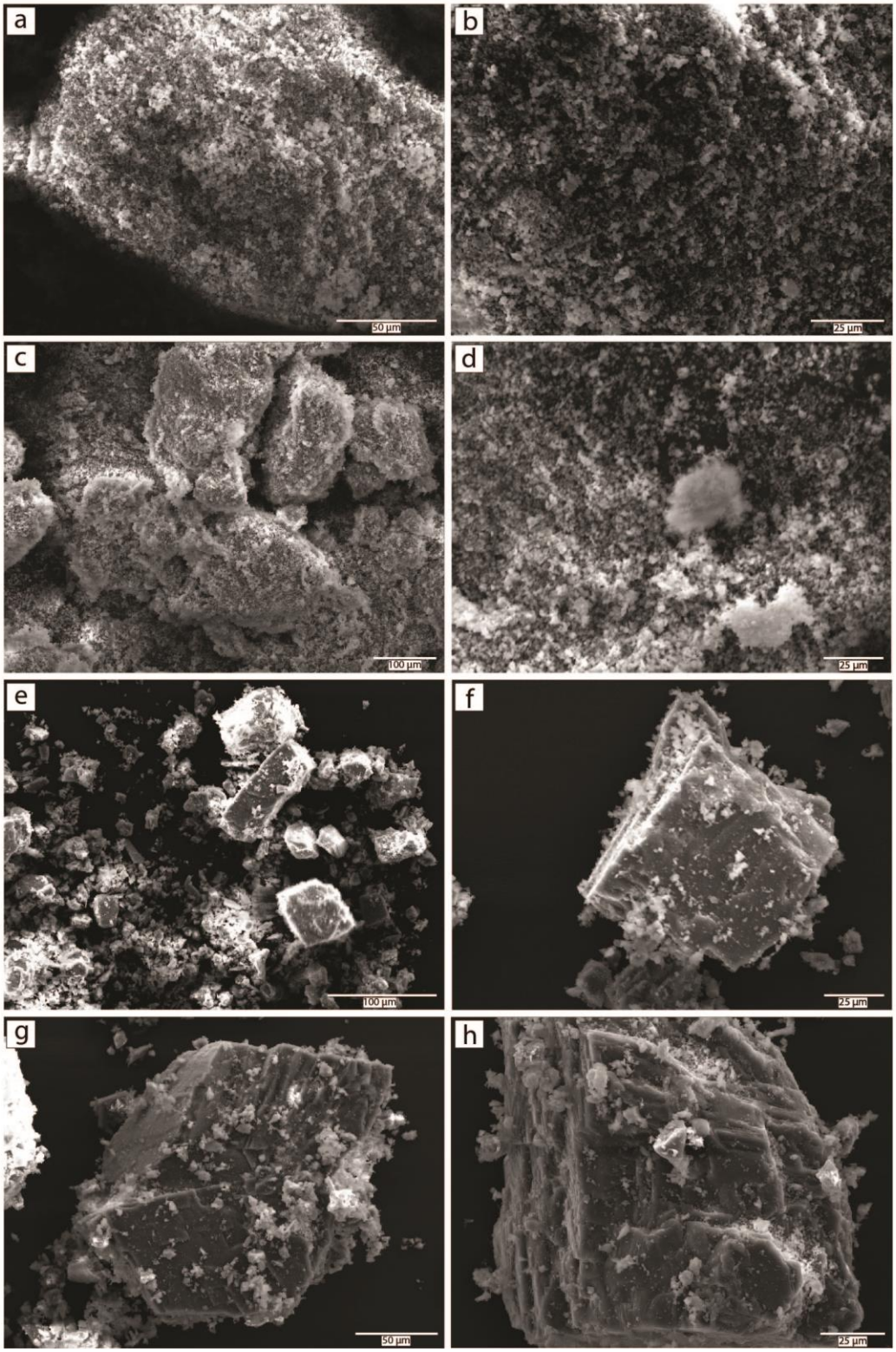

Figure 1: Backscatter electron (BSE) photographs of Rodolo and Sansa dolomites. (a, b) Unheated Rodolo sample showing a globular, very fine-grained texture, which provides high

surface area for isotope exchange and a potentially high internal water content. (c, d) Rodolo dolomite heated at 480 °C for 96h, showing no difference to the unheated material. (e, f) Unheated Sansa sample showing a clear textural difference compared to Rodolo with a better crystallinity and compact and solid grains. Nonetheless, fine grained microcrystals are attached to the larger grains. (g, h) Sansa heated at 480 °C for 96h, showing no visual difference to the unheated material. This result suggests that recrystallization—if occurring at all—is minor.

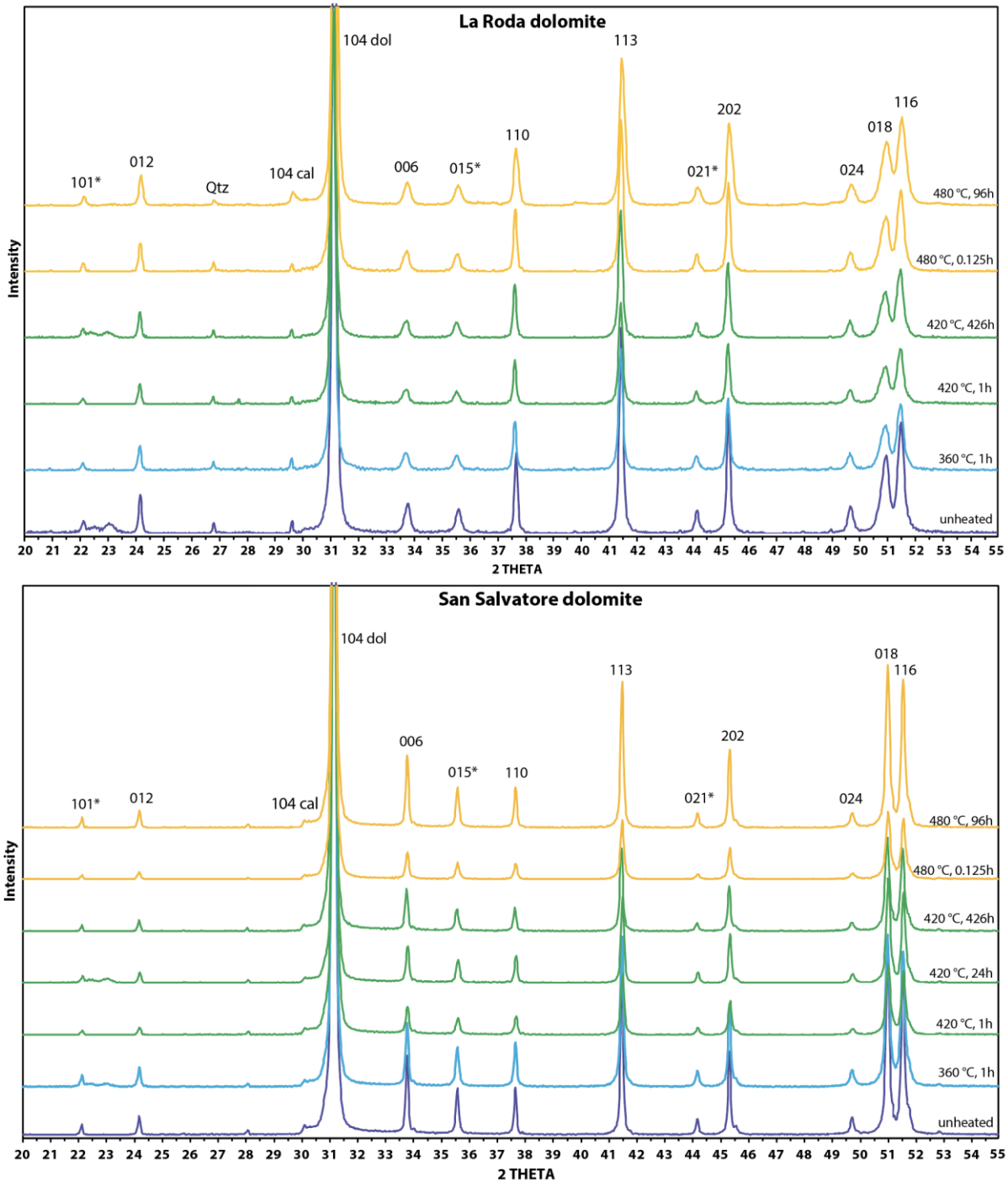

Figure 2: XRD patterns of Rodolo and Sansa dolomites unheated and at several experimental temperatures. 104 calcite peaks are visible in both samples throughout all experiments. Gregg et al. (2015) attribute the calcite 104 shift towards lower values to smaller crystallite sizes, in good agreement with our BSE observations (Figure 2). Intensities within experiments of the same material vary due sample mass limitations; still, this does not influence peak positions and ordering ratios.

3.2. Isotopic compositions

Unheated Rodolo dolomite is described by $\delta^{13}C$ = -3.73 ± 0.02 ‰ (VPDB), $\delta^{18}O$ = +2.78 ± 0.08 ‰ (VPDB), and Δ_{47} = 0.632 ± 0.012 ‰ (I-CDES, 95% CL; Table 1). Carbon and oxygen isotopes show an immediate shift towards lower values (reported as $\Delta\delta^{13}C$ and $\Delta\delta^{18}O$) by -0.10 ± 0.03 ‰ and -0.20 ± 0.11 ‰, respectively (Figure 3). The 480 °C, 96 h experiment exhibits the strongest isotope shift, with offsets of -0.29 ± 0.02 ‰ and -0.86 ± 0.09 ‰, respectively. Resulting Δ47 values decrease with increasing runtime and temperature; however, expected equilibrium Δ47 compositions are never reached in any experiment (Figure 4). When calculated at the longest runtime for each series, the absolute change in Δ47 relative to the unheated value (reported as $\Delta\Delta_{47}$) is: -0.119 ± 0.021 ‰ at 360 °C (168 h), -0.138 ± 0.020 ‰ at 420 °C (426 h), and -0.178 ± 0.021 ‰ at 480 °C (96 h). At all temperatures, Δ47 evolution is dominated by the immediate decrease at the beginning of the experiment. For example, calculated Δ47 temperatures rapidly increase to 41 ± 5 °C in the 360 °C experiments after 1h, which comprises ~80% of the total observed change across the entire experiment.

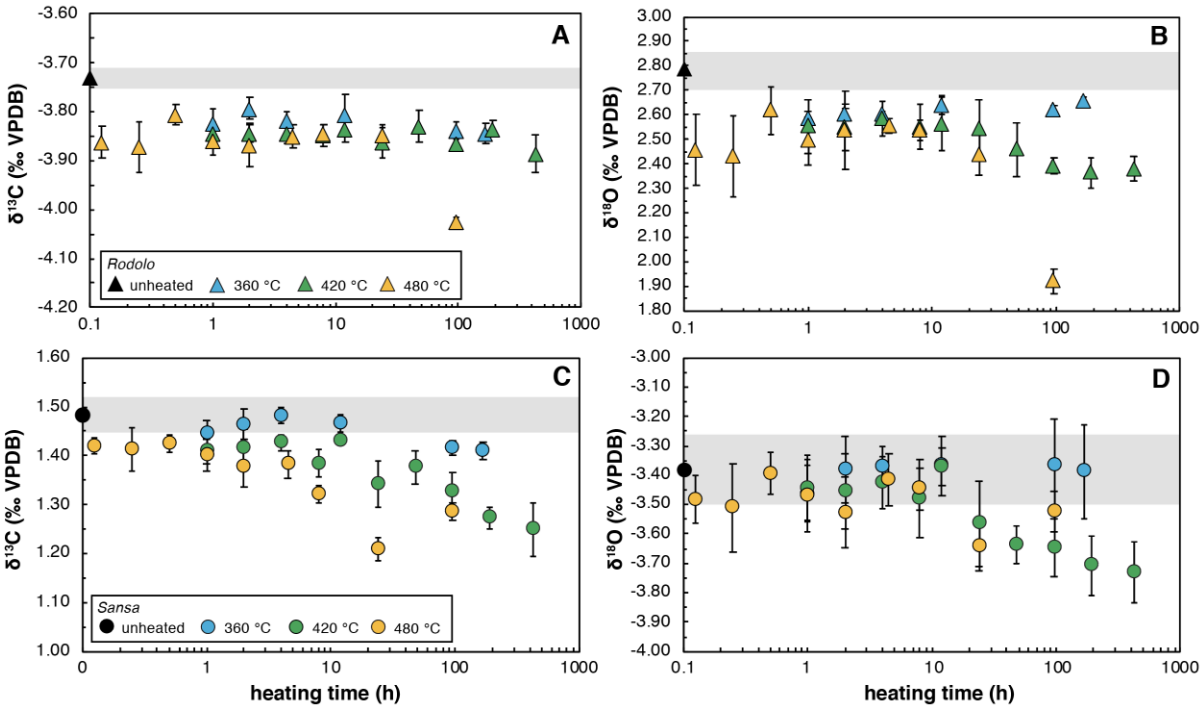

Figure 3: Sable isotope compositions of Rodolo (a, b) and Sansa (c, d) plotted as functions of heating time (logarithmic scale). There is an immediate shift toward lighter compositions in

Rodolo experiments, whereas Sansa exhibits a continuous decline for each temperature. For all panels: triangles = Rodolo, circles = Sansa. black = unheated material, blue = 360 °C, green = 420 °C, yellow = 480 °C. Uncertainties are ±1 sigma standard deviation and starting material uncertainty is grey. (Table 1).

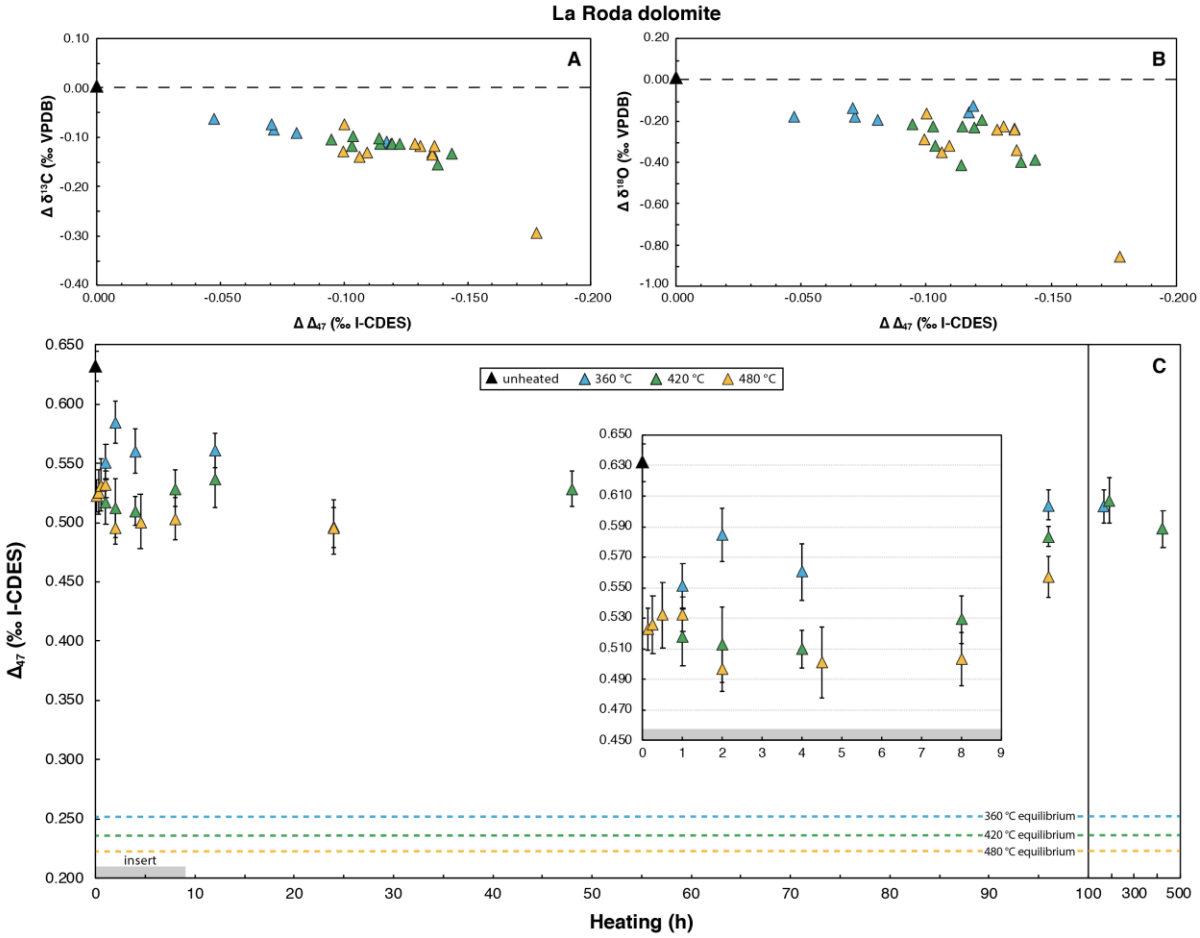

Figure 4: Rodolo dolomite change in (a) $\Delta\delta^{13}C$ and (b) $\Delta\delta^{18}O$ plotted against the $\Delta\Delta_{47}$, all relative to the unheated sample. (c) Clumped isotope evolution of Rodolo for the individual heating experiments. Uncertainties are 95% CL with equilibrium values plotted as dashed lines for each temperature after Anderson et al. (2021). For all panels: black = unheated, blue = 360 °C, green = 420 °C, yellow = 480 °C. The insert gives a detailed view on the first 9 hours of heating. Unertainties for (a) and (b) can be seen in Figure 3, and (c).

For San Salvatore, unheated isotope compositions are $\delta^{13}C$ = 1.48 ± 0.04 ‰ (VPDB), $\delta^{18}O$ = -3.38 ± 0.12 ‰ (VPDB), and Δ_{47} = 0.505 ± 0.013 ‰ (I-CDES, 95% CL). In contrast to Rodolo, the shift towards lighter compositions is not immediate, but happens gradually with heating time (Figure 3). The maximum $\Delta\delta^{13}C$ amount to -0.07 ± 0.04 ‰, -0.23 ± 0.06 ‰ and -0.27 ± 0.04 ‰, for 360, 420, and 480 °C, respectively. The $\Delta\delta^{18}O$ show a maximum change of -0.08 ± 0.20 ‰, -0.35 ± 0.16 ‰ and -0.26 ± 0.14 ‰ for 360, 420, and 480 °C, respectively.

Compared to Rodolo, where changes in $\delta^{18}O$ are larger than in $\delta^{13}C$, the magnitude of $\delta^{18}O$ and $\delta^{13}C$ changes are similar for Sansa. Similar to Rodolo, Δ_{47} values decrease with increasing temperature and runtime but never reach equilibrium (Figure 6c). Specifically, $\Delta\Delta_{47}$ are observed to be: -0.020 ± 0.018 ‰ at 360 °C (168 h), -0.099 ± 0.018 ‰ at 420 °C (192 h), and -0.100 ± 0.020 ‰ at 480 °C (96 h).

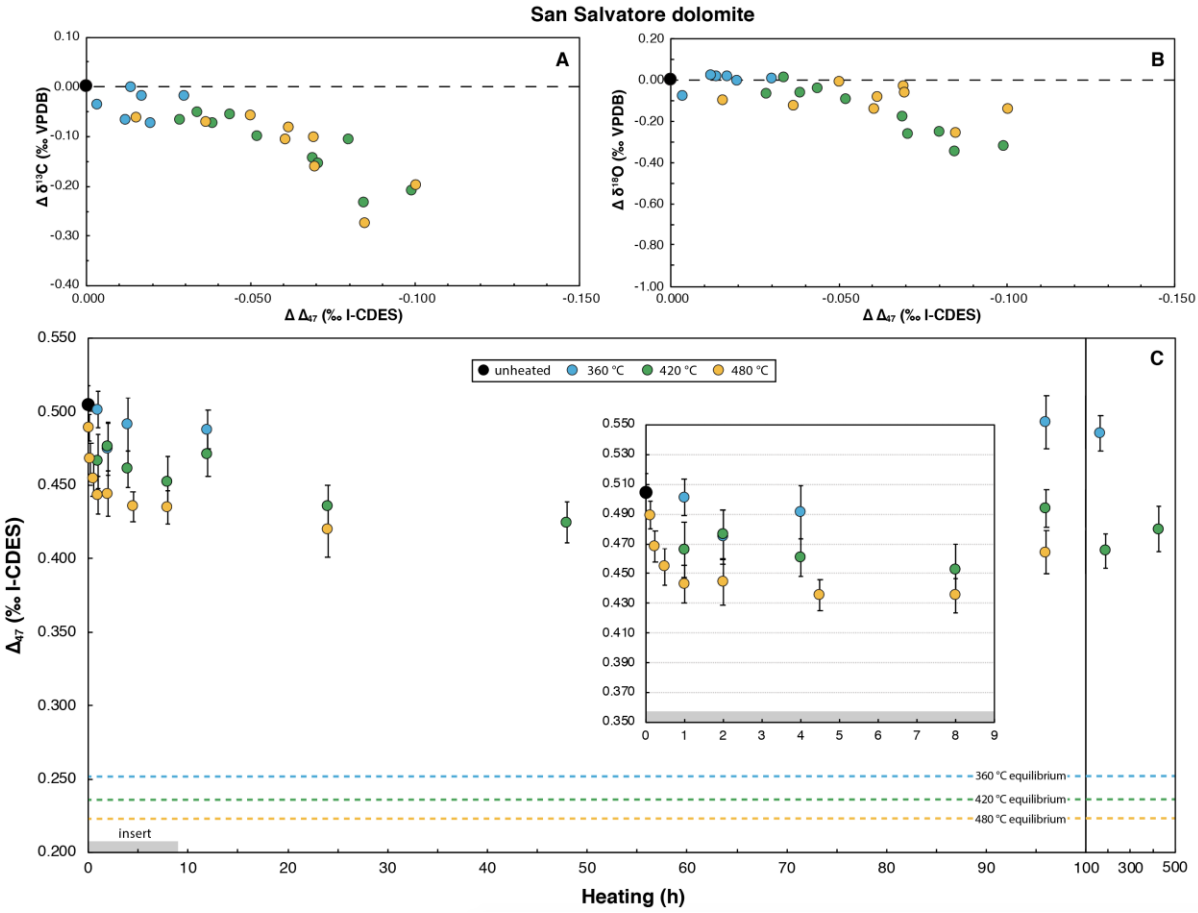

Figure 5: San Salvatore dolomite change in (a) $\Delta\delta^{13}C$ and (b) $\Delta\delta^{18}O$ plotted against $\Delta\Delta_{47}$, all relative to the unheated sample. (c) Clumped isotope evolution of Sansa for single heating experiments. Uncertainties are 95% CI with equilibrium values plotted as dashed lines for each temperature after Anderson et al. (2021). For all panels: black = unheated, blue = 360 °C, green = 420 °C, yellow = 480 °C. The insert gives a detailed view on the first 9 hours of heating. Uncertainties for (a) and (b) can be seen in Figure 3, and (c).

In summary, both dolomites show a trend towards lighter isotopic compositions with increasing temperature and runtime, but Rodolo changes rapidly at the beginning of each experiment, whereas Sansa shows a more gradual decrease and no detectable change within uncertainty at 360 °C. In Rodolo, $\delta^{18}O$ trends exhibit similar behavior as $\delta^{13}C$, with a -0.20 ± 0.11 ‰ and -0.10 ± 0.03 ‰ shift, respectively, and decrease at 360 °C after 1h. Unlike Rodolo, $\delta^{18}O$ values in the 360 °C series on Sansa are consistently identical to the initial composition

within uncertainty (Figure 3d). Although BSE images (Figure 1) and XRD patterns (Figure 2) display no clear evidence of recrystallization, we cannot exclude a small amount of decarbonation for Rodolo at 480°C and 96h runtime, as isotope values clearly diverge from the trend observed for shorter and colder experiments ($\Delta\delta^{13}C$ = -0.29 ± 0.02 ‰; $\Delta\delta^{18}O$ = -0.86 ± 0.09 ‰; Figure 4).

4 Discussion

Here, we first summarize our experimental results, discuss sample homogeneity in terms of stable isotope composition, and compare to results from the high-temperature Eugui dolomite of Lloyd et al. (2018). Next, we evaluate material-specific Arrhenius parameters using the HH21 disordered kinetic model for combined Eugui and Sansa dolomite results, and we discuss potential limitations when implementing the available data for the SE15 and He14 models. Finally, we argue for material-specific dolomite reordering kinetics, as has been advocated previously for calcite (Chen et al., 2019; Looser et al., 2023; Passey & Henkes, 2012), and we discuss the overall merits and limitations of reordering models for dolomite.

4.1 Stable isotope compositions and homogeneity of the starting materials

In the lacustrine Rodolo dolomite, we observe a rapid shift towards lower $\delta^{18}O$ and $\delta^{13}C$ values. Of particular interest is the initial drop in $\delta^{13}C$ by 0.10 ± 0.03 ‰ at 360 °C (Figure 3,4), after which $\delta^{13}C$ values do not resolvably change until heated to 480 °C for 96 h ($\Delta\delta^{13}C$ = -0.29 ± 0.02 ‰). In contrast, $\delta^{13}C$ values for the crystalline replacement Sansa dolomite change gradually within each temperature set, reaching values that are lower by -0.23 ± 0.06 ‰ and -0.27 ± 0.04 ‰ for the longest 420 °C and 480 °C runtimes (426 h and 96 h, respectively). Our fine-grained starting materials are homogeneous and exhibit standard deviations of ±0.04 and ±0.12 for $\delta^{13}C$ and $\delta^{18}O$, respectively (Rodolo: n = 13; Sansa: n = 11); thus, the observed changes exhibit a signal-to-noise ratio of ~5. In contrast, the unheated Eugui dolomite used for the reordering experiments by (Lloyd et al., 2018) is isotopically heterogeneous, with standard deviations of ±0.22 ‰ for $\delta^{13}C$ and ±1.02 ‰ for $\delta^{18}O$ (n = 35). The heterogeneity of this starting material was thus larger than any experimental changes observed here. Therefore, we suggest that similar shifts and trends in the experiments of Lloyd et al. (2018) may have gone undetected and cannot be excluded.

Previous calcite and aragonite heating studies observed constant $\delta^{13}C$ values throughout all experiments (Chen et al., 2019; Passey & Henkes, 2012; Stolper & Eiler, 2015); this has similarly been claimed for the dolomite heating experiments of Lloyd et al. (2018). Although most experimental heating studies make use of a CO2 atmosphere to track potential isotope exchange, the sensitivity of this approach is limited when experiments utilize large single crystals (i.e., mm size), as low S/V ratios render surficial diffusion processes negligible to the overall isotope signal. In principle, fine grained materials are more susceptible than larger grains to diffusional isotope exchange with CO2 at grain boundaries or to dissolution-reprecipitation processes, which can alter stable-isotope compositions. In fact, both of our fine-grained materials display such shifts towards lower $\delta^{13}C$ and $\delta^{18}O$ values, with a consistently faster and larger shift observed in the finer grained Rodolo dolomite relative to Sansa.

Whereas shifts in $\delta^{18}O$ of -0.2 to -0.6 ‰ have been detected in most calcite studies (Brenner et al., 2018; Henkes et al., 2014; Looser et al., 2023; Passey & Henkes, 2012), this is the first study observing a systematic trend in dolomite. There are several possibilities to exchange $\delta^{18}O$ within the experiment: (i) exchange between dolomite and the CO2 atmosphere, (ii) exchange between dolomite and intra-crystalline H2O, (iii) exchange between dolomite and H2O derived from silver oxalate. Because of the high S/V ratio, it is possible that diffusional isotope exchange with CO2 could happen in both of our starting materials. However, we only observe a rapid drop in Rodolo, whereas Sansa is constant within uncertainty (± 0.12 ‰) for the first few hours of heating (Figure 3). It has to be expected that after 100+ hours of heating time at 360 to 480 °C an oxygen isotope fractionation between CO2 and carbonates will take place (Deines, 2004; Schauble et al., 2006; Horita, 2014). Yet, diffusional isotope exchange is unlikely to happen within minutes of heating. Thus, we suggest that in the Rodolo experiments, exchange with intra-crystalline water could play a more important role. Intra-crystalline water cannot be removed before the experiments and could react with the dolomite upon heating. The presence of up to 2.5 % intracrystalline water in synthetic protodolomites has been reported by (Kelleher & Redfern, 2002; Zheng et al., 2021). Assuming the intra-crystalline fluid of Rodolo has a similar composition as the fluid it precipitated from ($\delta^{18}O$ (VSMOW) of 2.60 ± 0.85 ‰ calculated from the fluid $\delta^{18}O$ equation of Anderson et al. 2021), one percent of the total oxygen pool consisting of intra-crystalline fluid could explain the immediate shift by -0.20 ± 0.11 ‰, if it fully exchanged with dolomite upon heating (Unheated Rodolo $\delta^{18}O$(VSMOW) = 33.78 ‰). In scenario (iii), if H2O from the silver oxalate ($\delta^{18}O$ (VSMOW) = 32.15 ± 0.09 ‰) would account for 1% of the total oxygen pool in the experimental charge, it would result in a maximum change of 0.01 ‰, which is within analytical uncertainty. In an extreme case, if we assume $\delta^{18}O$ of -20 ‰ for the oxalate-water, the dolomite could shift by -0.6 ‰.

The cause of observed $\delta^{13}C$ decreases remains unclear. We propose that the decrease in $\delta^{13}C$ —especially for Rodolo—results from surficial isotope exchange between CO_2, and CO_3^{2-} in dolomite, as described previously ((Deines, 2004; Schauble et al., 2006; Horita, 2014). These studies show a $^{13}C/^{12}C$ fractionation of 2-5 ‰ between CO_2 and dolomite/calcite at our experimental temperatures, with CO_2 being enriched and dolomite/calcite becoming depleted in ^{13}C. Unfortunately, we cannot verify if a ^{13}C enrichment in CO_2 occurred since post-experimental CO_2 was not measured in our experiments.

In summary, grain size and texture seem to have a significant role on the susceptibility to isotopic modification in the experiments. The fine grained or micro crystalline texture of Rodolo provides a high S/V, possibly enhancing stable isotope fractionation of oxygen and carbon. Intra-crystalline water, may have a significant impact on the rapid oxygen isotope shift, but carbon isotope fractionation can only be explained with an exchange with the CO_2 atmosphere. However, the reason for the rapid carbon isotope shift in Rodolo remains unclear. The stable isotopic depletion in the Sansa experiments is gradual, suggesting that intra-crystalline water is absent and the fractionation is dominated by the exchange with the CO_2 atmosphere. Detailed studies of the water content of protodolomite are necessary to demonstrate its importance.

4.2. Comparison of Δ_{47} reordering in different dolomites

To directly compare our Δ_{47} results, which are reported in the I-CDES scale, with those of Lloyd et al. (2018), we converted their data to the CDES 90°C by adding 0.092 ‰ to each value (Bonifacie et al., 2017; Lloyd et al., 2018). One fundamental difference between Rodolo, Sansa, and Eugui is their formation temperature and thus their initial Δ_{47} values (Figure 6). Eugui is described by $\Delta_{47} = 0.360 \pm 0.014$ ‰, which corresponds to a formation temperature of 163 ± 6 °C (Anderson et al., 2021b), in good agreement with fluid inclusion-based estimates of 160-175 °C ((Velasco et al., 1987). In contrast, Rodolo and Sansa are described by $\Delta_{47} = 0.632 \pm 0.012$ ‰ and 0.505 ± 0.013 ‰ (13 ± 4 and 61 ± 6 °C, respectively; Anderson et al. 2021 calibration), much further from equilibrium Δ_{47} at the experimental temperatures (Figures 4,5,6). Nevertheless, we observe similar Δ_{47} changes for Sansa and Eugui dolomites at a given temperature, whereas Rodolo Δ_{47} shifts are roughly 0.050 ‰ larger at all temperatures (Figure 6, Table 1). This larger shift results from the fact that Rodolo Δ_{47} mostly decreases prior to the first experimental timepoint of 1 hour at 360 and 420 °C and 7.5 minutes at 480 °C; thus, the exact timing of this decrease is not resolvable with the available data. The contrasting behavior between samples manifests best in the 360 °C experiments, where Rodolo shows a ~0.100 ‰ larger Δ_{47} decrease than Sansa after 1h, meaning that 30 % of the reordering progress in the Rodolo dolomite is already achieved by this point (Figure 5,6). In contrast, better ordered and coarser grained dolomites are largely resistant to bond reordering at such temperatures, as can be seen in the Sansa experiment at 360 °C.

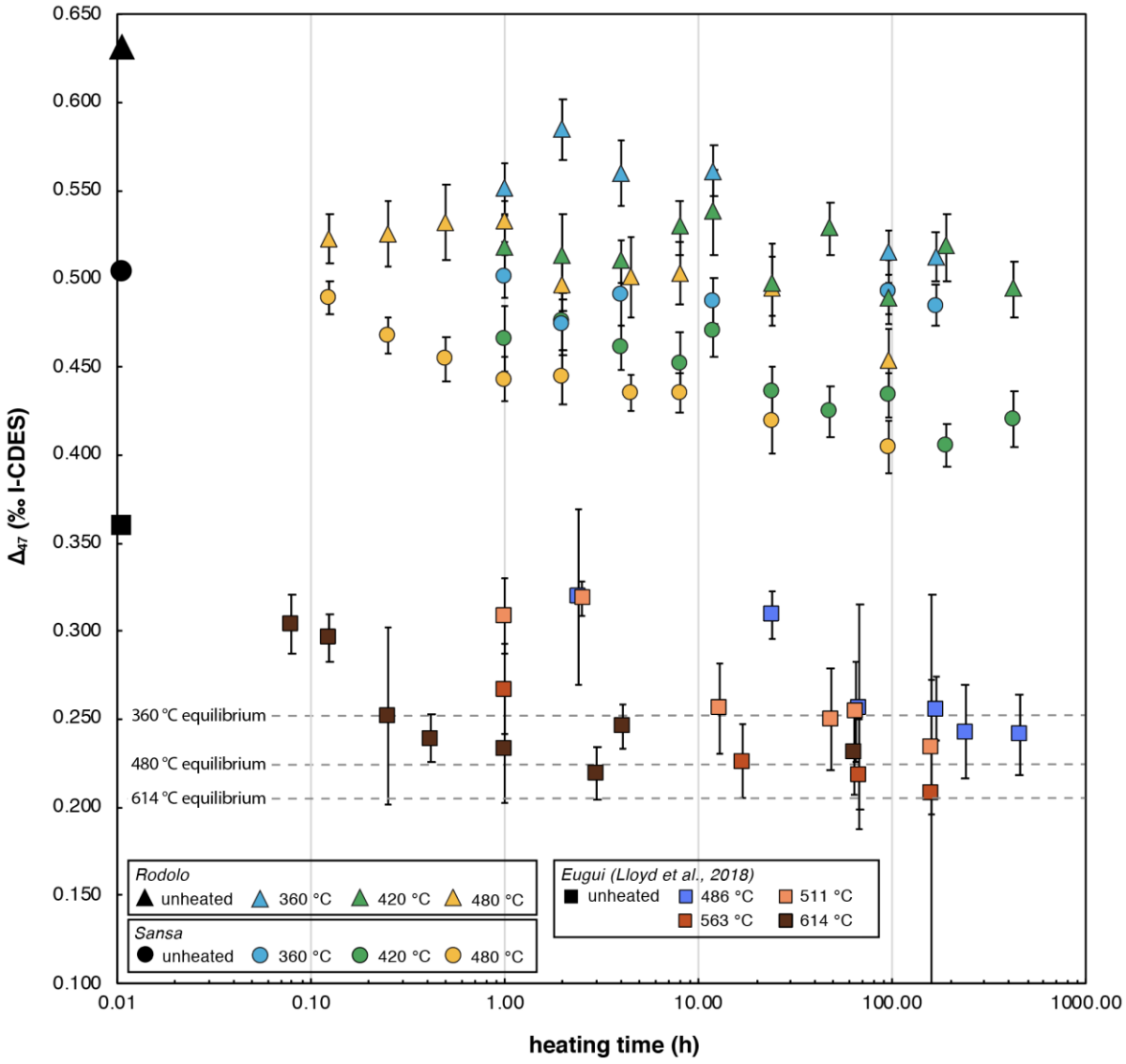

586

587 **Figure 6:** Δ_{47} vs logarithmic heating time. Triangles = Rodolo, circles = Sansa, squares = Eugui.
588 Starting materials are in black, and uncertainty is given as 95% CI. Note that Eugui dolomite
589 experiments reach equilibrium (within uncertainty) whereas Rodolo and Sansa never approach
590 equilibrium in any experiment.
591

592 Figure 6 shows a comparison of all available dolomite experiment Δ_{47} results with the
593 exception of the 409, 460, and 717 °C experiments of Lloyd et al. (2018), as these only reported
594 two (409 °C and 460 °C) or three (717 °C) time points, which is insufficient to quantify reaction
595 kinetics (Hemingway and Henkes, 2021). For Rodolo and Sansa, the 360 °C experiments
596 converge to similar values after ~100h of heating. However, 480 °C experiments for these
597 samples never converge but rather evolve along trends with identical slopes (-0.011 ‰/hour) that
598 are separated roughly by 0.05 ‰ (yellow symbols in Figure 6); this 0.05 ‰ difference coincides
599 with the magnitude of the rapid initial drop in Rodolo. The changes observed in Eugui ($\Delta\Delta_{47}$ = -
600 0.119 ± 0.027 ‰ at 486 °C) and Sansa ($\Delta\Delta_{47}$ = -0.100 ± 0.020 ‰ at 480 °C) are statistically

identical, with the Sansa experiments displaying slightly higher temporal resolution and lower uncertainty than Eugui. Unlike Sansa or Rodolo, the Eugui experiments all reach their respective equilibrium temperature within uncertainty (95 % CI). Given the difference in starting material grain size, we expected that reordering would proceed faster and to a larger extent in Sansa and especially Rodolo relative to Eugui, However, this was not observed (Figure 7).

Combined, these results imply that stoichiometric and poorly ordered dolomite first experiences an initial annealing step after which it behaves similarly to well-ordered dolomite upon further heating, independent of grain size, S/V ratio, and, importantly, of the fact that crystallographic ordering remains low. Therefore, grain size and crystallographic ordering state do not appear to play a significant role for Δ_{47} reordering reactions after the initial annealing step, but seem to increase the rate of $\delta^{13}C$ and, especially, $\delta^{18}O$ modification under the used experimental conditions (section 4.1). However, the changes in bulk composition observed under the chosen experimental conditions cannot easily be extrapolated to natural diagenetic conditions. This is because the experimental conditions here represent extreme cases of temperature exposure (e.g 25 to 360+ °C in seconds) while in natural systems a gradual temperature increase over geological timescales to such temperatures would almost certainly be accompanied by recrystallization (Ryan et al., 2022).

In general, after the initial shift, all three dolomites follow similar reordering trajectories. The fundamental difference is the approach to equilibrium, which is reached only by Eugui, i.e., the dolomite that was already formed at high temperature and thus starts closest to equilibrium experimental temperatures (Figure 6). As the distance from equilibrium should be the main driving force controlling Δ_{47} reordering rate (Passey and Henkes, 2012), it is somewhat surprising that the two dolomites with initial Δ_{47} values further from equilibrium do not experience a larger Δ_{47} shift than Eugui at a given temperature. Experiments on much longer timescales are necessary to better understand this behavior. Possible interpretations include: (i) that the first rapid decrease in Δ_{47} is not related to bond reordering but to some other mechanism, and (ii) that following this initial step change, the reordering rate is much slower than predicted by current models. Either interpretation would imply that dolomite is more resistant to solid-state reordering than is currently predicted by any reordering model. Alternatively, there could be a second step in the reordering behavior where the kinetics of reaction increase again, i.e. a three-step behavior as opposed to a two-step behavior as observed in calcite. This second step has not been reached in the experiments because they were of too short duration. If such a second step is involved, this would require a delayed and lower activation energy process which initiates only after a certain amount of time at elevated temperatures (exceeding our experimental series). A similar change in solid-state reordering was described for calcite after the transition from aragonite (Chen et al., 2019).

4.3. Influence of crystallographic ordering on stable isotope fractionation and Δ_{47} solid state bond reordering upon initial heating.

The temperature vs. Δ_{47} calibrations of (Bonifacie et al., 2017) and (Müller et al., 2019) for dolomite did not show a measurable difference in equilibrium Δ_{47} values between well-ordered and disordered dolomite. Our experiments, however, show that the poorly ordered Rodolo is initially more susceptible than Sansa to $\square^{13}C$, $\square^{18}O$, and Δ_{47} modification upon heating (Figure 3, 4). Based on the model of (Lippmann, 1973), the ordered dolomite unit cell has alternating planes of Ca^{2+}- CO_3^{2-}- Mg^{2+} - CO_3^{2-} . Poorly ordered dolomite such as Rodolo

will contain irregular alternation of Mg and Ca planes, or planes with mixed Ca and Mg ions (Ogasawara et al., 1981), leading to a lower crystal lattice stability due to elevated internal strain when compared to ordered dolomite (Sibley, 1990). Despite a large change in Δ_{47}, ordering does not significantly increase in any Rodolo experiment, except for a small increase from 0.31 to 0.36 (±0.03) at 480 °C heating for 96h (Table 1). This indicates that heating, at these relatively short timescales, only significantly influences the carbonate ion groups but not the cation ordering. The study of (Zheng et al., 2021) showed that heating times of 2 months at temperature of 200 and 300 °C lead to increased ordering in protodolomite, but still far from perfect ordering, whereas heating at 100°C did not lead to a measurable increase in cation ordering. This shows that the kinetics of reordering are indeed very slow and suggests that much longer experiments are necessary for a better understanding of a possible effect of cation reordering on the kinetics of clumped isotope reordering.

The small grainsize and high S/V ratio of Rodolo could be the cause of an increased exchange due to the larger surface area, possibly also hosting increased amounts of intra-crystalline water. Moreover, cation disorder in an unordered crystal lattice could lead to an increased diffusion rate due to lattice defects, and internal strain leading to enhanced exchange of O and C isotopes. After this initial change, however, the cation disorder and the smaller grain size does not seem to influence the Δ_{47} reordering rates and isotope exchange compared to well-ordered dolomites. With the available data it is not possible to provide a conclusive explanation for the rapid drop in Δ_{47} observed in Rodolo. Nonetheless, the implications of this observation are that poorly ordered dolomites in nature could undergo a first step of bond reordering before the temperature is sufficiently high to initiate cation ordering. Indeed, all studies reporting dolomite clumped isotope temperatures colder than about 50 to 60 °C are from dolomites with poor ordering and/or that are non-stoichiometric and calcium rich (Baldermann et al., 2020; Murray & Swart, 2017; Ryan et al., 2022; Ryb & Eiler, 2018; Veillard et al., 2019).

For Δ_{47} solid state bond reordering, this implies that in a stoichiometric, well-ordered dolomite, Δ_{47} evolution can be accurately described with solid-state bond reordering models (Hemingway & Henkes, 2021; Henkes et al., 2014; Stolper & Eiler, 2015). In disordered or non-stoichiometric dolomite, this evolution might be initially influenced by isotope exchange between CO_2, H_2O, and the CO_3^{2-} ion. Although the specific process involved remains unclear, it potentially influences the initial composition of the dolomite; thus, current models would not be directly applicable. More experiments on unordered dolomite and/or high magnesium calcite are needed to better characterize potential influence of isotope exchange resulting from crystallographic order-disorder and/or grainsize and S/V.

4.4. Dolomite reordering kinetics

Quantifying Δ_{47} reordering Arrhenius parameters is crucial when applying clumped isotopes to geological questions. In this section, we implement our results within existing solid-state bond reordering models (He14, SE15 and HH21) using the "*isotopylog*" package for Python 3.7 (Hemingway, 2020) to derive reaction kinetics at each temperature. We then use these results to update dolomite Arrhenius parameters in Section 4.5.

Model fits for Sansa and Rodolo at each temperature are shown in Figure 8. For all three models, the small Δ_{47} change for 360 °C heating experiments in Sansa leads to low signal/noise ratios (i.e., S/N < 3); thus, derived kinetic parameters at this temperature are highly uncertain.

Overall, the HH21 model appears to fit all Rodolo experiments better than the SE15 and He14 models, as evidenced by the slightly lower model vs. data root-mean-square error (rmse) values. However, rmse for all models and all experiments is near analytical uncertainty. Thus, with the available data, it is not conclusive to endorse or reject a specific model. More experiments with longer runtimes and higher temperatures are needed to refine model fits and reduce uncertainties.

Still, current experiments and model fits provide two valuable insights on the trajectories of reordering kinetics in the different dolomites: (i) Rodolo fits with the HH21 model "bottoms out" after ~40% of reaction at all temperatures. In contrast, the SE15 model predicts a steady first-order decline towards equilibrium values. Because of the high S/V ratio in Rodolo, diffusional barriers for carbonate groups are low; thus, such carbonate pairs could diffuse through the crystal lattice until equilibrium values are attained or the material recrystallizes. Longer experiments are required to conclusively determine which model behavior is more accurate. (ii) Sansa experimental data can be better described by Arrhenuis kinetics than Rodolo for two reasons. First, they are not complicated by the initial ~0.05 ‰ drop of unknown mechanistic origin observed for Rodolo. Second, they display faster and more complete reactions with increasing temperature, as predicted.

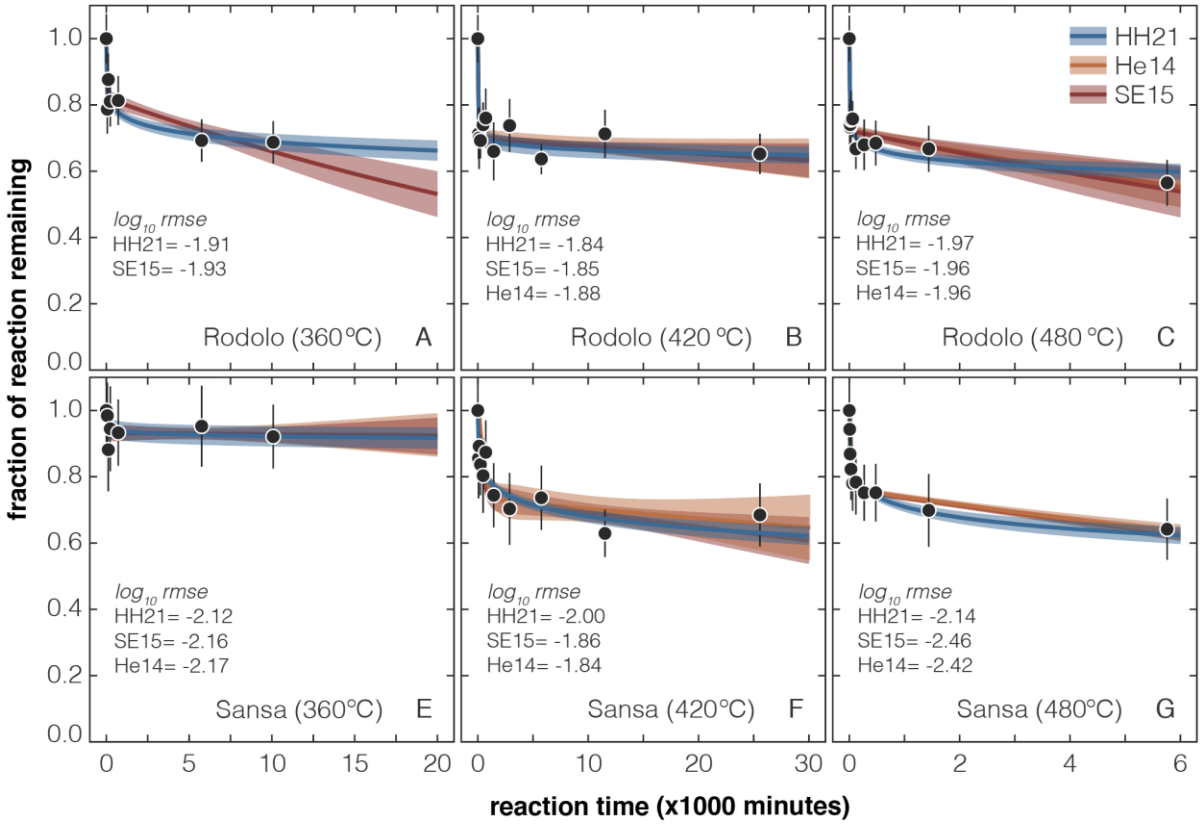

Figure 7: Rodolo and Sansa heating experiments with model fits of Hemingway and Henkes (2021) (HH21 – blue lines), Stolper and Eiler (2015) (SE21 – red lines), and Henkes et al. (2014) (He14 – orange lines). Single experiments are black circles and uncertainties are reported as 95 % CL; Shaded areas represent ±1 std.dev. model uncertainty; The y-axis, fraction of reaction

remaining shows the reaction progress towards equilibrium values, 1.0 = unreacted, 0.0 =equilibrated. Fit statistics for each model are given as $\log_{10}$ rmse (root mean square error) in each box.

In contrast to Rodolo—where Δ_{47} reordering "flattens out" after the initial drop at all experimental temperatures—Sansa displays a more continuous Δ_{47} evolution, as expected from Arrhenian kinetics. From these Δ_{47} evolution fits, it becomes clear that the initial reaction mechanisms differ between the two dolomites. As described in sections 4.2 and 4.3, we suggest that this different behavior results from enhanced diffusion due to a combination of higher S/V ratios and crystallographic disorder of dolomite and possibly the presence of intracrystalline water in poorly ordered protodolomite. However, disorder only appears to influence initial Δ_{47} reordering behaviour; after this initial decrease, Rodolo—although remaining disordered—behaves similarly to the well-ordered Eugui and Sansa samples. Therefore, cation disordering per se does not seem to be a dominant factor controlling observed kinetic differences between dolomite types.

Since both experimental series must be extended with additional temperature sets, it is not possible to obtain Arrhenius fits for Rodolo or Sansa alone (Table S1, Figures S2-S5). This is especially true for Rodolo, since bottoming out at ~60% reaction remaining for all temperatures is fundamentally inconsistent with Arrhenius kinetics. Nevertheless, Sansa Arrhenian kinetics can be combined with Eugui data from Lloyd et al. (2018) to provide improved "dolomite average" Arrhenian parameters.

4.5. Arrhenius parameters for well-ordered dolomite vs. calcite

To obtain more robust kinetic parameters and compare our data with those of Lloyd et al. (2018), we use selected Sansa and Eugui heating experiment results to derive combined Arrhenius parameters. We specifically include results for Sansa at 420 and 480 °C and for Eugui at 486, 511, 563, and 614 °C. Because Lloyd et al. (2018) do not report kinetic parameters for individual heating experiments, we cannot calculate combined Sansa and Eugui Arrhenius results for the He14 and SE15 models; we therefore limit our discussion to HH21 model predictions.

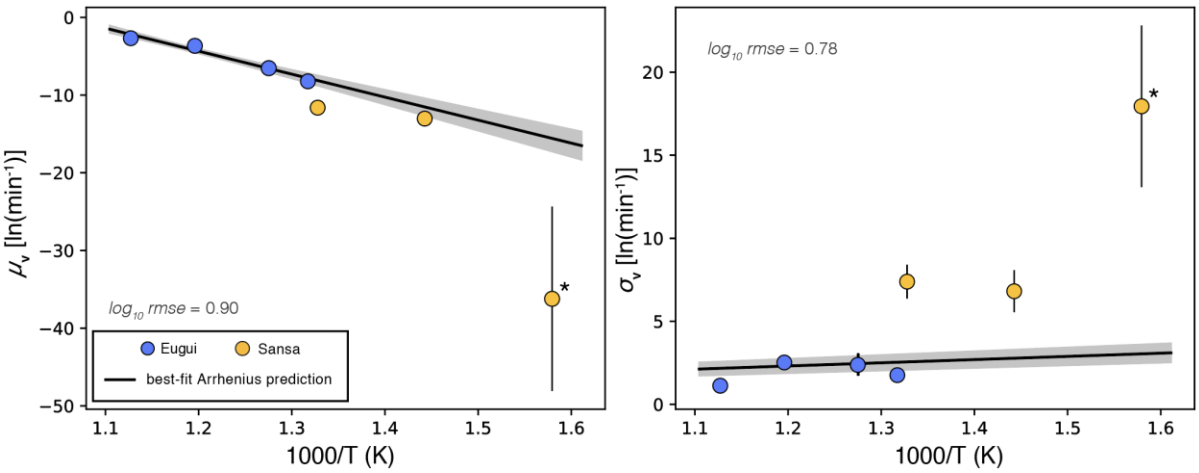

Figure 8: Arrhenius parameter plots combining the Eugui data from the original HH21 manuscript with Sansa and Rodolo. Model mis-fits are given as $\log_{10}$ rmse (root mean square error). The Sansa 360 °C experimental data is not included in the regression, but illustrates the lack of reaction and high uncertainties at low temperature.

Combined Arrhenius parameters for Eugui (486 – 614 °C) and Sansa (420 – 480 °C) dolomites using the HH21 model display a mean activation energy μ_E of 246 ± 35.4 kJ mol^{-1} (±1σ). This is in good agreement to the 230.3 ± 47.7 kJ mol^{-1} (±1 std. dev.) values originally calculated from Hemingway and Henkes (2021) using only the Eugui data. Arrhenius pre-exponential factors are also within error with ν_0 = 31.2 ± 5.1 min^{-1} for the combined calculation and ν_0 = 29.0 ± 6.8 min^{-1} for Eugui alone. The activation energy width (σ_E) for the combined and Eugui-only regressions also overlap within uncertainty (Table 2).

Table 2: Arrhenius energy distributions using the HH21 disordered kinetic model. The Data for Eugui dolomite from Lloyd et al. (2018) and calcite average is directly from Hemingway and Henkes (2021). Belemninte cc from heating experiments of (Looser et al., 2023).

Samples	$\boldsymbol{\mu_E}$ kJmol^{-1}	$\boldsymbol{\nu_0}$ min^{-1}	$\boldsymbol{\sigma_E}$ kJmol^{-1}	**n**
Sansa+Eugui	246.0 ± 35.4	31.2 ± 5.1	16.0 ± 2.8	6
Eugui	230.3 ± 47.7	29.0 ± 6.8	14.8 ± 2.2	4
calcite average	224.3 ± 27.6	31.5 ± 4.6	17.4 ± 0.7	24
belemnite cc	167.7 ± 12.3	25.6 ± 2.2	21.6 ± 2.8	4

Compared to average values of all previously measured calcite materials, the combined kinetic parameters of Sansa and Eugui display a higher mean activation energy (μ_E = 246 ± 35.4 kJ mol^{-1} and 224.3 ± 27.6 kJ mol^{-1}, dolomite and calcite respectively) but almost identical Arrhenius pre-exponential factors (ν_0 = 31.2 ± 5.1 and 31.5 ± 4.6 min^{-1}, dolomite and calcite respectively). However, (Hemingway & Henkes, 2021) provide a range of activation energies for optical, brachiopod, and spar calcite, which span from μ_E = 247.4 ± 15.6 to 290.2 ± 27.1 kJ mol^{-1}, and ν_0 = 34.2 ± 2.3 to 42.7 ± 4.6 min^{-1}. If compared to this data, the combined dolomite parameters show activation energies on the lower end of the carbonate range. The activation energy distribution width for combined dolomite is σ_E = 16.0 ± 2.8 kJ mol^{-1}, within the range of different calcite materials (σ_E = 13.5 ± 2.7 to 24.3 ± 0.8 kJ mol^{-1}). This suggests that the distribution of O-O bond distances in calcite and dolomite are described by similar variance, despite differences (if any) in μ_E and ν_0 between these materials (Hemingway & Henkes, 2021).

Similar experiments were carried out by (Looser et al., 2023), which compared optical calcite to belemnite calcite reordering rates. The results show that the belemnite has a significantly lower activation energy of μ_E = 167 ± 12.3 kJ mol^{-1}, compared to the average calcite of μ_E = 224.3 ± 27.6 kJ mol^{-1}. Activation energy distributions in calcite are material specific (this thesis chapter 3) and Δ_{47} temperature histories can be modelled to a satisfying precision using such material specific parameters. This is in contrast to dolomite. Primary precipitated and pristine dolomite (Rodolo), if heated, cannot be described by available reordering models because neither of them can describe the first step in Δ_{47}.

To evaluate the potential behavior of disordered dolomite, we derive activation energies for this initial drop by only using the first three (at 420 and 480 °C) and four (360 °C) experimental data points of the Rodolo series. The calculated activation energies μ_E of 108 ± 21 kJ mol^{-1} and ν_0 = 13 ± 4 (rmse = 0.24, HH21 model, Figure 9) for the initial Δ_{47} step indicate that pristine dolomite is highly susceptible to reordering and is almost instantaneously modified if exposed to heating or burial.

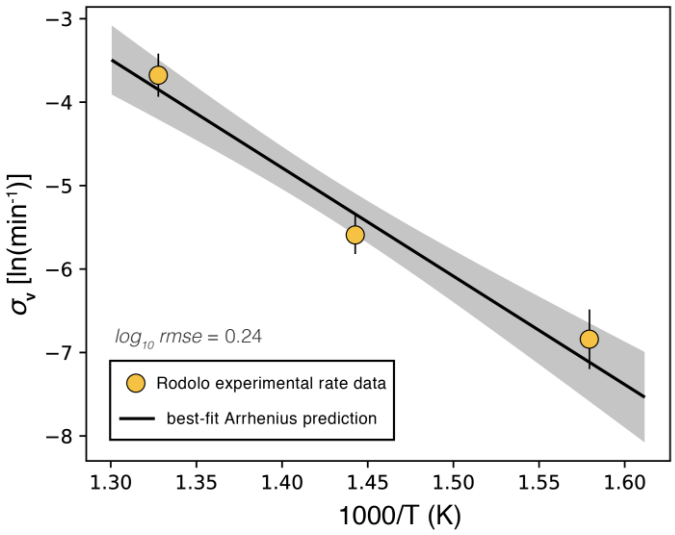

Figure 9: Rodolo Arrhenius parameter plot describing the initial drop. Data points used here are: unheated, 1h, 2h, 4h at 360 °C; unheated, 1h, 2h for 420 °C, and unheated, 0.125h, 0.25h at 480 °C.

4.6. Using the Sansa+Eugui combined kinetic parameters for assessing Δ_{47} temperatures of a replacive dolomite from the Eastern Jura Mountains

In this case study, we apply the Sansa+Eugui combined dolomite parameters to a real geological system and by comparing predicted vs. measured reordering for a replacive dolomite with a well-constrained burial history evaluate if Δ_{47} temperatures result from solid-state bond reordering or recrystallization during burial.

The dolomite in this case study originates from the Carnian (~237-227 Ma) Gansingen Member (Klettgau Formation, Jordan et al., 2016) in the Eastern Jura Mountains of Switzerland. It is a microcrystalline replacive dolomite with a low cation ordering ratio of 0.5 (Fig. 11). Dolomitization of the originally calcareous sediment took place soon after deposition as indicated by closed ostracod shells only partially filled with dolomicrite (Wildi, 1976). Samples were collected from the reference section of the Gansingen Member in the claypit Frick (Swiss coord.: LV95: 2643000/1261900; Jordan et al., 2016). At this location, Looser al. (2022) reconstructed a detailed burial history for the Early Jurassic sedimentary succession using

combined clumped isotopes and U-Pb dating of diagenetic carbonate cements and partially reordered fossils. In their work, these authors confirmed the burial temperature estimates of a previous study by Mazurek et al. (2006) and also revealed a temperature anomaly during Late Jurassic and Early Cretaceous with peak burial temperatures of ~104°C for a duration in the range between 1 and 31 Ma.

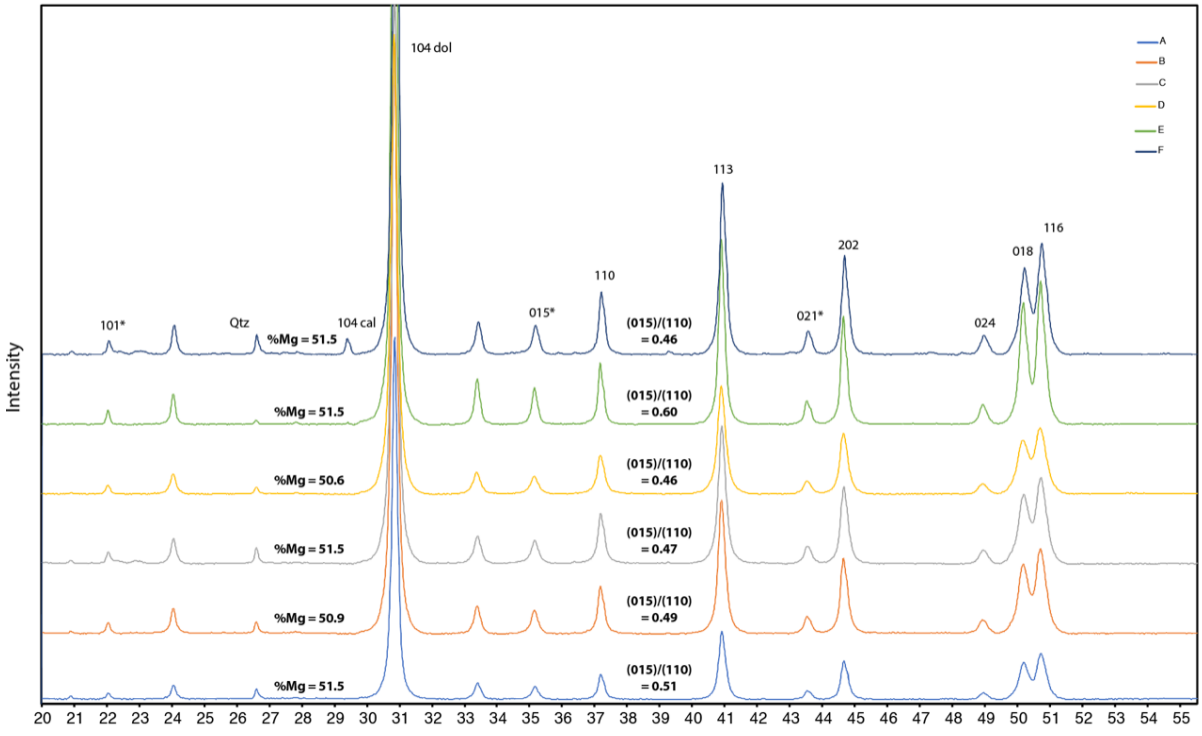

Figure 10: XRD patterns of the six Gansingen Dolomite samples.

The Δ_{47} of the Gansingen Dolomite was determined on six samples yielding values within error of each other and a pooled Δ_{47} temperature of 44 ± 3°C using I-CDES scale and the Anderson et al. 2021 calibration (Table S2). Notably, this temperature is higher than expected for early-diagenetic replacement dolomitization, especially given the fact that the Gansingen Dolomite at Frick remained at very shallow (< 50 m) burial until Early Jurassic (Jordan et al., 2016; Reisdorf et al., 2011). The elevated Δ_{47} temperatures can potentially be explained by different scenarios which are tested using the Sansa+Eugui combined dolomite parameters together with the burial history of Looser (2022). In the first scenario, originally lower Δ_{47} temperatures reflecting the early-diagenetic replacement dolomitization were modified by solid-state reordering caused by high burial temperatures during Late Jurassic-Early Cretaceous. The second scenario involves recrystallization of the original early replacive dolomite at a later point in time with the measured Δ_{47} temperatures reflecting ambient burial temperatures during the recrystallization event.

We estimate the temperature during early-diagenetic replacement dolomitization to 30-36°C by using the dolomite-water oxygen isotope fractionation equation of Vasconcelos et al. (2005) together with the dolomite $\delta^{18}O$ of -1.55 ‰ V-PDB, and assuming a $\delta^{18}O$ of the dolomitizing fluid between -1 and 0 ‰ V-SMOW, reflecting the brackish to marine depositional environment of the Gansingen Member (Jordan et al. 2016). The results are presented in Figure 12. Based on the model predictions, peak burial temperatures of 104°C for 1 Ma (Figures 12a), 16Ma (Figures 12b), and 31 Ma (Figures 12c) cause no change in Δ_{47} temperatures due to reordering. Accordingly, the elevated Δ_{47} temperatures cannot be explained by solid-state reordering alone and instead suggest recrystallization at a later point in time. Based on the thermal history of Looser et al. (2022), this recrystallization would have taken place during Early Jurassic, at 185-175 Ma.

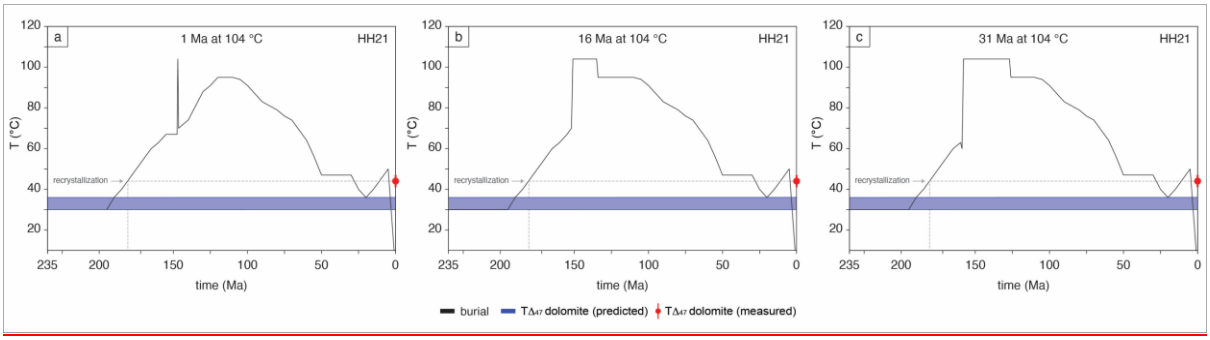

Figure 11: Predicted change in calcite Δ_{47} temperatures (blue) resulting from the experienced burial history (black). a) Peak burial temperatures of 104°C for 1Ma. b) Peak burial temperatures of 104°C for 16Ma and c) 31Ma. Precipitation of the dolomite takes place at 235 Ma during the Carnian with subsequent burial. The range of possible Δ_{47} temperatures between 44 ± 3°C (I-CDES, Anderson 2021 calibration) and 53 ± 3°C (CDES, Müller 2019 calibration) is indicated with red dots on each diagram. Initial temperatures during early-diagenetic dolomitization is in the range of 30 and 36 °C as constrained by the average $\delta^{18}O$ (VPDB) and seawater $\delta^{18}O$ of -1 to 0 ‰.

4.7. Limitations to the application of dolomite Δ_{47} data in natural systems

In this study, we provide experimental evidence that early diageneitic (proto)dolomite is less resistant to solid state bond reordering, and more susceptible to isotopic modification when exposed to elevated temperatures than well-ordered dolomite. Even though our experimental temperatures by far exceed diagenetic and burial temperatures, the results agree with Ryan et al. (2022) who showed that even if recrystallization is not clearly detected, Δ_{47} temperatures in early diagenetic dolomites can be altered to higher temperatures during shallow burial. Following the initial step to ~50 °C, which is potentially happening in many mimetic and/or pristine primary and poorly ordered dolomites at shallow burial (Ryan et al., 2022; Winkelstern & Lohmann, 2016), dolomite reordering can be described with solid state bond reordering models using dolomite specific kinetic parameters (section 4.5).

Although we have derived Arrhenius parameters for this first step (Figure 9), an application of such is not recommended because the link between these "first step parameters" and "combined dolomite parameters" (Figure 8 and 9) is not adequately constrained without additional experiments. Whether the observed temperature in the Gansinger dolomite is due to micro-recrystallization or pure solid-state reordering remains inconclusive. More experiments at lower temperatures and shorter time intervals are needed.

In summary, Δ_{47} temperatures of pristine primary dolomite, such as Rodolo, are likely trustworthy and may reflect the original temperature of formation. However, secondary dolomites showing Δ_{47}-temperatures between 40 and 60 °C, are very likely recrystallized to some extend and do not display the original temperature of dolomitization (Ryan et al., 2022; Winkelstern & Lohmann, 2016). Thus, reconstructions of temperatures of dolomitization should be taken with caution and the general applicability of reordering models on dolomites displaying ~50 °C Δ_{47} is uncertain, if the dolomitization temperature is the parameter of interest. There is a need for more heating experiments on primary/pristine dolomite to accurately describe the first step of Δ47 temperature annealing observed here and elsewhere (Ryan et al., 2022; Winkelstern & Lohmann, 2016).

5 Conclusions

This study provides a set of experiments on two distinct stoichiometric dolomite materials. In addition to published data on dolomite reordering (Lloyd et al., 2018), we show that specific dolomite types have a distinct behavior upon heating.

The poorly ordered La Roda dolomite displays significant and very rapid stable isotope- and Δ_{47} alteration upon heating, which cannot be reliably described with any available reordering model. Although we did not observe signs of recrystallization or decarbonation, and there is no increase in cation ordering, an alteration of the original isotope composition is observed. We suggest that this rapid change in Δ_{47} temperature and stable isotope composition is a function of grain size, S/V ratio and cation ordering. We derived activation energies for this first alteration step which are low enough to rapidly change the Δ_{47} temperature to a value of ~50 °C even in shallowest burial scenarios. Such a behaviour is in good agreement with studies of Winkelstern and Lohmann (2016) and Ryan et al. (2022) showing an increased Δ_{47} in early diagenetic dolomites spite of very shallow burial.

The well-ordered San Salvatore dolomite (Sansa) lacks this immediate shift upon heating and shows a slight gradual depletion in stable isotope compositions and a well-defined Δ_{47} evolution upon heating and increasing runtime. We combine our results for San Salvatore dolomite with previously published results from Lloyd et al. (2018), to derive robust kinetic reordering parameters using the disordered kinetic model by Hemingway and Henkes (2021). Dolomite parameters show a higher activation energy compared to the calcite average, but compare within uncertainty in Arrhenius pre-exponential factor, and activation energy distribution width.

We suggest that the new reordering kinetic parameters from this study can be applied to geologic scenarios which involve a crystalline or non-mimetic dolomite type. However, dolomite temperatures of such samples may not record the original dolomitization temperature, but rather a temperature of early diagenetic recrystallization, as shown in the case study of the Gansingen

dolomite. In the case of pristine dolomite such as the La Roda dolomite, the initial process leading to the rapid depletion upon heating needs further investigation.

Acknowledgments

We thank Madalina Jaggi, Stewart Bishop, Lydia Zehnder for assistance in the laboratory. The research was founded by Swiss National Science Foundation grants 200021_169849 to SMB and 200020_166153 to MWS. The authors declare no financial conflict of interest.

Open Research

Upon acceptance of the manuscript, all replicate-level clumped isotope data of samples and standards from which all data included in this study can be derived will be submitted to the EarthChem database and this section will replaced with specific instructions on how to access the data shown here.

.

References

Anderson, N. T., Kelson, J. R., Kele, S., Daëron, M., Bonifacie, M., Horita, J., et al. (2021). A unified clumped isotope thermometer calibration (0.5–1100°C) using carbonate-based standardization. *Geophysical Research Letters*, 1–11. https://doi.org/10.1029/2020gl092069

Antao, S. M., Mulder, W. H., Hassan, I., Crichton, W. A., & Parise, J. B. (2004). Cation disorder in dolomite, CaMg(CO3)2, and its influence on the aragonite + magnesite ↔ dolomite reaction boundary. *American Mineralogist*, *89*(7), 1142–1147. https://doi.org/10.2138/am-2004-0728

Arvidson, R. S., & Mackenzie, F. T. (1999). The dolomite problem: Control of precipitation kinetics by temperature and saturation state. *American Journal of Science*, *299*(4), 257–288. https://doi.org/10.2475/ajs.299.4.257

Baldermann, A., Mittermayr, F., Bernasconi, S. M., Dietzel, M., Grengg, C., Hippler, D., et al. (2020). Fracture dolomite as an archive of continental palaeo-environmental conditions. *Communications Earth & Environment*, *1*(1), 1–12. https://doi.org/10.1038/s43247-020-00040-3

Bernasconi, S. M., Daëron, M., Bergmann, K. D., Bonifacie, M., Meckler, A. N., Affek, H. P., et al. (2021). InterCarb: A Community Effort to Improve Interlaboratory Standardization of the Carbonate Clumped Isotope Thermometer Using Carbonate Standards. *Geochemistry, Geophysics, Geosystems*, *22*(5), 1–25. https://doi.org/10.1029/2020GC009588

942 Bonifacie, M., Calmels, D., Eiler, J. M., Horita, J., Chaduteau, C., Vasconcelos, C., et al. (2017).
943 Calibration of the dolomite clumped isotope thermometer from 25 to 350 °C, and
944 implications for a universal calibration for all (Ca, Mg, Fe)CO3carbonates. *Geochimica*
945 *et Cosmochimica Acta*, *200*, 255–279. https://doi.org/10.1016/j.gca.2016.11.028

946 Brauchli, M., McKenzie, J. A., Strohmenger, C. J., Sadooni, F., Vasconcelos, C., & Bontognali,
947 T. R. R. (2016). The importance of microbial mats for dolomite formation in the Dohat
948 Faishakh sabkha, Qatar. *Carbonates and Evaporites*, *31*(3), 339–345.
949 https://doi.org/10.1007/s13146-015-0275-0

950 Brenner, D. C., Passey, B. H., & Stolper, D. A. (2018). Influence of water on clumped-isotope
951 bond reordering kinetics in calcite. *Geochimica et Cosmochimica Acta*, *224*, 42–63.
952 https://doi.org/10.1016/j.gca.2017.12.026

953 Brenner, D. C., Passey, B. H., Holder, R. M., & Viete, D. R. (2021). Clumped-Isotope
954 Geothermometry and Carbonate U–Pb Geochronology of the Alta Stock Metamorphic
955 Aureole, Utah, USA: Insights on the Kinetics of Metamorphism in Carbonates.
956 *Geochemistry, Geophysics, Geosystems*, *22*(4), 1–21.
957 https://doi.org/10.1029/2020GC009238

958 Came, R. E., Eiler, J. M., Veizer, J., Azmy, K., Brand, U., & Weidman, C. R. (2007). Coupling
959 of surface temperatures and atmospheric CO2 concentrations during the Palaeozoic era.
960 *Nature*, *449*(7159), 198–201. https://doi.org/10.1038/nature06085

961 Chen, S., Ryb, U., Piasecki, A. M., Lloyd, M. K., Baker, M. B., & Eiler, J. M. (2019).
962 Mechanism of solid-state clumped isotope reordering in carbonate minerals from
963 aragonite heating experiments. *Geochimica et Cosmochimica Acta*, *258*, 156–173.
964 https://doi.org/10.1016/j.gca.2019.05.018

965 Coplen, T. B. (2011). Guidelines and recommended terms for expression of stable-isotope-ratio
966 and gas-ratio measurement results. *Rapid Communications in Mass Spectrometry*, *25*(17),
967 2538–2560. https://doi.org/10.1002/rcm.5129

968 Deines, P. (2004). Carbon isotope effects in carbonate systems. *Geochimica et Cosmochimica*
969 *Acta*, *68*(12), 2659–2679. https://doi.org/10.1016/j.gca.2003.12.002

970 Dennis, K. J., & Schrag, D. P. (2010). Clumped isotope thermometry of carbonatites as an
971 indicator of diagenetic alteration. *Geochimica et Cosmochimica Acta*, *74*(14), 4110–
972 4122. https://doi.org/10.1016/j.gca.2010.04.005

973 Eiler, J. M. (2011). Paleoclimate reconstruction using carbonate clumped isotope thermometry.
974 *Quaternary Science Reviews*, *30*(25–26), 3575–3588.
975 https://doi.org/10.1016/j.quascirev.2011.09.001

976 Fernandez, A., Müller, I. A., Rodríguez-Sanz, L., van Dijk, J., Looser, N., & Bernasconi, S. M.
977 (2017). A Reassessment of the Precision of Carbonate Clumped Isotope Measurements:
978 Implications for Calibrations and Paleoclimate Reconstructions. *Geochemistry,*
979 *Geophysics, Geosystems*, *18*(12). https://doi.org/10.1002/2017GC007106

980 Garcia Del Cura, M. A., Calvo, J. P., Ordonez, S., Jones, B. F., Canaveras, J. C., Garc??a Del
981 Cura, M. A., et al. (2001). Petrographic and geochemical evidence for the formation of
982 primary, bacterially induced lacustrine dolomite: La Roda “white earth” (Pliocene,

Central Spain). *Sedimentology*, *48*(4), 897–915. https://doi.org/10.1046/j.1365-3091.2001.00388.x

Ghosh, P., Adkins, J., Affek, H., Balta, B., Guo, W., Schauble, E. A., et al. (2006). 13C-18O bonds in carbonate minerals: A new kind of paleothermometer. *Geochimica et Cosmochimica Acta*, *70*(6), 1439–1456. https://doi.org/10.1016/j.gca.2005.11.014

Goldsmith, J. R., & Graf, D. L. (1958). Structural and Compositional Variations in Some Natural Dolomites. *The Journal of Geology*, *66*(6), 678–693. https://doi.org/10.1086/626547

Graf, D., & Goldsmith, J. R. (1955). Dolomite—magnesian calcite relations at elevated temperatures and CO2 pressures. *Geochimica et Cosmochimica Acta*, *7*(3–4).

Gregg, J. M., Bish, D. L., Kaczmarek, S. E., & Machel, H. G. (2015). Mineralogy, nucleation and growth of dolomite in the laboratory and sedimentary environment: A review. *Sedimentology*, 1749–1769. https://doi.org/10.1111/sed.12202

Hemingway, J. D. (2020). isotopylog: open-source tools for clumped isotope kinetic data analysis.

Hemingway, J. D., & Henkes, G. A. (2021). A disordered kinetic model for clumped isotope bond reordering in carbonates. *Earth and Planetary Science Letters*, *566*. https://doi.org/10.1016/j.epsl.2021.116962

Henkes, G. A., Passey, B. H., Grossman, E. L., Shenton, B. J., P??rez-Huerta, A., & Yancey, T. E. (2014). Temperature limits for preservation of primary calcite clumped isotope paleotemperatures. *Geochimica et Cosmochimica Acta*, *139*, 362–382. https://doi.org/10.1016/j.gca.2014.04.040

Horita, J. (2014). Oxygen and carbon isotope fractionation in the system dolomite-water-CO2 to elevated temperatures. *Geochimica et Cosmochimica Acta*, *129*, 111–124. https://doi.org/10.1016/j.gca.2013.12.027

Hu, B., Radke, J., Schlüter, H. J., Heine, F. T., Zhou, L., Bernasconi, S. M., et al. (2014). A modified procedure for gas-source isotope ratio mass spectrometry: The long-integration dual-inlet (LIDI) methodology and implications for clumped isotope measurements. *Rapid Communications in Mass Spectrometry*, *28*(13), 1413–1425. https://doi.org/10.1002/rcm.6909

Jendrzejewski, N., Trull, T. W., Pineau, F., & Javoy, M. (1997). Carbon solubility in Mid-Ocean Ridge Basaltic melt at low pressures (250-1950 bar). *Chemical Geology*, *138*(1–2), 81–92. https://doi.org/10.1016/S0009-2541(96)00176-3

John, C. M., & Bowen, D. (2016). Community software for challenging isotope analysis: First applications of ???Easotope??? to clumped isotopes. *Rapid Communications in Mass Spectrometry*, *30*(21), 2285–2300. https://doi.org/10.1002/rcm.7720

Jordan, P., Pietsch, J. S., Bläsi, H., Furrer, H., Kündig, N., Looser, N., et al. (2016). The middle to late Triassic Bpaänkerjoch and Klettgau formations of northern Switzerland. *Swiss Journal of Geosciences*, *109*(2), 257–284. https://doi.org/10.1007/s00015-016-0218-3

Kelleher, I. J., & Redfern, S. A. T. (2002). Hydrous calcium magnesium carbonate, a possible precursor to the formation of sedimentary dolomite. *Molecular Simulation*, *28*(6–7), 557–572. https://doi.org/10.1080/08927020290030134

Lippmann, F. (1973). Crystal Chemistry of Sedimentary Carbonate Minerals. In *Sedimentary Carbonate Minerals* (Vol. 35, pp. 5–96). Berlin, Heidelberg: Springer Berlin Heidelberg. https://doi.org/10.1007/978-3-642-65474-9_2

Lloyd, M. K., Eiler, J. M., & Nabelek, P. I. (2017). Clumped isotope thermometry of calcite and dolomite in a contact metamorphic environment. *Geochimica et Cosmochimica Acta*, *197*, 323–344. https://doi.org/10.1016/j.gca.2016.10.037

Lloyd, M. K., Ryb, U., & Eiler, J. M. (2018). Experimental calibration of clumped isotope reordering in dolomite. *Geochimica et Cosmochimica Acta*, *242*, 1–20. https://doi.org/10.1016/j.gca.2018.08.036

Looser, N, Madritsch, H., Guillong, M., Laurent, O., Wohlwend, S., & Bernasconi, S. M. (2021). Absolute Age and Temperature Constraints on Deformation Along the Basal Décollement of the Jura Fold-and-Thrust Belt From Carbonate U-Pb Dating and Clumped Isotopes. *Tectonics*, *40*(3), 1–17. https://doi.org/10.1029/2020TC006439

Looser, Nathan. (2022). *Coupling Clumped Isotope Thermometry and U-Pb Dating of Carbonates for Applications in Stratigraphy, Diagenesis, and Geodyamics*. Zürich. https://doi.org/10.3929/ethz-b-000554116

Looser, Nathan, Petschnig, P., Hemingway, J. D., Fernandez, A., Grafulha Morales, L., Perez-Huerta, A., et al. (2022). Clumped Isotope Reordering in Belemnite and Optical Calcites: Towards Material- Specific Reordering Kinetics. *SSRN Electronic Journal*, 1–54. https://doi.org/10.2139/ssrn.4152167

Lugli, S., Torres-Rutz, J., Garuti, G., & Olmedo, F. (2000). Petrography and Geochemistry of the Eugui Magnesite Deposit (Western Pyrenees, Spain): Evidence for the Development of a Peculiar Zebra Banding by Dolomite Replacement. *Economic Geology*, *95*(8), 1775. https://doi.org/10.2113/gsecongeo.95.8.1775

Lumsden, D. N. (1979). X-ray Analysis Quantative X-Ray Analysis, *49*(2), 0–6.

Lumsden, D. N., & Chimahusky, J. S. (1980). Relationship between Dolomite Nonstoichiometry and Carbonate Facies Parameters. In *Concepts and Models of Dolomitization* (pp. 123–137). SEPM Society for Sedimentary Geology. https://doi.org/10.2110/pec.80.28.0123

Machel, H. G. (2004). Concepts and models of dolomitization: a critical reappraisal. *Geological Society, London, Special Publications*, *235*(1), 7–63. https://doi.org/10.1144/GSL.SP.2004.235.01.02

Manche, C. J., & Kaczmarek, S. E. (2021). A global study of dolomite stoichiometry and cation ordering through the phanerozoic. *Journal of Sedimentary Research*, *91*(5), 520–546. https://doi.org/10.2110/JSR.2020.204

Martinez, I., Zhang, J., & Reeder, R. J. (1996). In situ X-ray diffraction of aragonite and dolomite at high pressure and high temperature; evidence for dolomite breakdown to aragonite and magnesite. *American Mineralogist*, *81*(5–6), 611–624. https://doi.org/10.2138/am-1996-5-608

Meckler, A. N., Ziegler, M., Mill??n, M. I., Breitenbach, S. F. M., Bernasconi, S. M., Millán, M. I., et al. (2014). Long-term performance of the Kiel carbonate device with a new

correction scheme for clumped isotope measurements. *Rapid Communications in Mass Spectrometry*, *28*(15), 1705–1715. https://doi.org/10.1002/rcm.6949

Millán, M. I., Machel, H., & Bernasconi, S. M. (2016). Constraining Temperatures of Formation and Composition of Dolomitizing Fluids In the Upper Devonian Nisku Formation (Alberta, Canada) With Clumped Isotopes. *Journal of Sedimentary Research*, *86*(2), 107–112. https://doi.org/10.2110/jsr.2016.6

Müller, I. A., Violay, M. E. S., Storck, J.-C. C., Fernandez, A., van Dijk, J., Madonna, C., & Bernasconi, S. M. (2017). Clumped isotope fractionation during phosphoric acid digestion of carbonates at 70 °C. *Chemical Geology*, *449*, 1–14. https://doi.org/10.1016/j.chemgeo.2016.11.030

Müller, I. A., Rodriguez-Blanco, J. D., Storck, J.-C., do Nascimento, G. S., Bontognali, T. R. R., Vasconcelos, C., et al. (2019). Calibration of the oxygen and clumped isotope thermometers for (proto-)dolomite based on synthetic and natural carbonates. *Chemical Geology*, *525*(July), 1–17. https://doi.org/10.1016/j.chemgeo.2019.07.014

Murray, S. T., & Swart, P. K. (2017). Evaluating Formation Fluid Models and Calibrations Using Clumped Isotope Paleothermometry on Bahamian Dolomites. *Geochimica et Cosmochimica Acta*, *206*, 73–93. https://doi.org/10.1016/j.gca.2017.02.021

Nooitgedacht, C. W., van der Lubbe, H. J. L. L., Ziegler, M., & Staudigel, P. T. (2021). Internal Water Facilitates Thermal Resetting of Clumped Isotopes in Biogenic Aragonite. *Geochemistry, Geophysics, Geosystems*, *22*(5), 1–13. https://doi.org/10.1029/2021gc009730

Ogasawara, Y., Ochida, E., & Imai, N. (1981). Thermochemical Recalculation for Thermal DissociationEquilibrium of Dolomite-Thermochemical Studies in the System CaO-MgO-SiO2-CO2-H2O. *Bulletin of Science and Engineering Resealch Laboratory Waseda University*, *95*, 15–26.

Passey, B. H., & Henkes, G. A. (2012). Carbonate clumped isotope bond reordering and geospeedometry. *Earth and Planetary Science Letters*, *351–352*, 223–236. https://doi.org/10.1016/j.epsl.2012.07.021

Pina, C. M., Pimentel, C., & Crespo, Á. (2020). Dolomite cation order in the geological record. *Chemical Geology*, *547*, 119667. https://doi.org/10.1016/j.chemgeo.2020.119667

Reeder, R. J., & Wenk, H. R. (1983). Structure refinements of some thermally disordered dolomites. *American Mineralogist*, *68*(7–8), 769–776. https://doi.org/10.1128/CMR.00045-07

Reisdorf, A. G., & Wetzel, A. (2018). Evidence for synsedimentary differential tectonic movements in a low-subsidence setting: Early Jurassic in northwestern Switzerland. *Swiss Journal of Geosciences*, *111*(3), 417–444. https://doi.org/10.1007/s00015-018-0318-3

Reisdorf, A. G., Wetzel, A., Schlatter, R., & Jordan, P. (2011). The Staffelegg Formation: A new stratigraphic scheme for the Early Jurassic of northern Switzerland. Swiss Journal of Geosciences (Vol. 104). https://doi.org/10.1007/s00015-011-0057-1

Ryan, B. H., Kaczmarek, S. E., Rivers, J. M., & Manche, C. J. (2022). Extensive recrystallization of Cenozoic dolomite during shallow burial: A case study from the Palaeocene–Eocene Umm er Radhuma formation and a global meta-analysis. *Sedimentology*, *69*(5), 2053–2079. https://doi.org/10.1111/sed.12982

Ryb, U., Lloyd, M. K. K., Stolper, D. A. A., Eiler, J. M. M., Ryb U., Lloyd M.K., Stolper D.A., E. J. M., Ryb, U., et al. (2017). The clumped-isotope geochemistry of exhumed marbles from Naxos, Greece. *Earth and Planetary Science Letters*, *470*, 1–12. https://doi.org/10.1016/j.epsl.2017.04.026

Ryb, Uri, & Eiler, J. M. (2018). Oxygen isotope composition of the Phanerozoic ocean and a possible solution to the dolomite problem. *Proceedings of the National Academy of Sciences*, *115*(26), 6602–6607. https://doi.org/10.1073/pnas.1719681115

Schauble, E. A., Ghosh, P., & Eiler, J. M. (2006). Preferential formation of 13C-18O bonds in carbonate minerals, estimated using first-principles lattice dynamics. *Geochimica et Cosmochimica Acta*, *70*(10), 2510–2529. https://doi.org/10.1016/j.gca.2006.02.011

Schmid, T. W., & Bernasconi, S. M. (2010). An automated method for "clumped-isotope" measurements on small carbonate samples. *Rapid Communications in Mass Spectrometry*, *24*(14), 1955–1963. https://doi.org/10.1002/rcm.4598

Shenton, B. J., Grossman, E. L., Passey, B. H., Henkes, G. A., Becker, T. P., Laya, J. C., et al. (2015). Clumped isotope thermometry in deeply buried sedimentary carbonates: The effects of bond reordering and recrystallization. *Bulletin of the Geological Society of America*, *127*(7–8), 1036–1051. https://doi.org/10.1130/B31169.1

Sibley, D. F. (1990). Unstable to stable transformations during dolomitization. *The Journal of Geology*, *98*(5), 739–748.

Steinfink, H., & Sans, F. J. (1959). Refinement of the crystal structure of dolomite*. *American Mineralogist*, *44*(5–6), 679–682. https://doi.org/10.1080/0305724750050110

Stolper, D. A., & Eiler, J. M. (2015). The kinetics of solid-state isotope-exchange reactions for clumped isotopes: A study of inorganic calcites and apatites from natural and experimental samples. *American Journal of Science*, *315*(5), 363–411. https://doi.org/10.2475/05.2015.01

Vasconcelos, C., & McKenzie, J. A. (1997). Microbial mediation of modern dolomite precipitation and diagenesis under anoxic conditions (Lagoa Vermelha, Rio de Janeiro, Brazil). *Journal of Sedimentary Research*, *67*(3), 378–390. https://doi.org/10.1306/D4268577-2B26-11D7-8648000102C1865D

Vasconcelos, C., McKenzie, J. A., Warthmann, R., & Bernasconi, S. M. (2005). Calibration of the ??18O paleothermometer for dolomite precipitated in microbial cultures and natural environments. *Geology*, *33*(4), 317–320. https://doi.org/10.1130/G20992.1

Veillard, C. M. A., John, C. M., Krevor, S., & Najorka, J. (2019). Rock-buffered recrystallization of Marion Plateau dolomites at low temperature evidenced by clumped isotope thermometry and X-Ray diffraction analysis. *Geochimica et Cosmochimica Acta*, *252*, 190–212. https://doi.org/10.1016/j.gca.2019.02.012

Velasco, F., Pesquera, A., Arce, R., & Olmedo, F. (1987). A contribution to the ore genesis of the magnesite deposit of Eugui, Navarra (Spain). *Mineralium Deposita*, *22*(1), 33–41. https://doi.org/10.1007/BF00204241

Vickers, M. L., Fernandez, A., Hesselbo, S. P., Price, G. D., Bernasconi, S. M., Lode, S., et al. (2020). Unravelling Middle to Late Jurassic palaeoceanographic and palaeoclimatic signals in the Hebrides Basin using belemnite clumped isotope thermometry. *Earth and Planetary Science Letters*, *546*, 116401. https://doi.org/10.1016/j.epsl.2020.116401

Vickers, M. L., Bernasconi, S. M., Ullmann, C. V, Lode, S., Looser, N., Morales, L. G., et al. (2021). Marine temperatures underestimated for past greenhouse climate. *Scientific Reports*, *11*(1), 1–9. https://doi.org/10.1038/s41598-021-98528-1

Warren, J. (2000). Dolomite: occurrence, evolution and economically important associations. *Earth-Science Reviews*, *52*(1–3), 1–81. https://doi.org/10.1016/S0012-8252(00)00022-2

Wildi, W. (1976). Die Molluskenfauan des Gansinger Dolomites (Trias , Karnian , Mittlerer Keuper) im aargauischen Tafeljura (Nordschweiz) Die Molluskenfauna des Gansinger Dolomites. *Eclogae Geologicae Helvetiae*, *69*(3), 671–684.

Winkelstern, I. Z., & Lohmann, K. C. (2016). Shallow burial alteration of dolomite and limestone clumped isotope geochemistry. *Geology*, *44*(6), 467–470. https://doi.org/10.1130/G37809.1

Winkelstern, I. Z., Kaczmarek, S. E., Lohmann, K. C., & Humphrey, J. D. (2016). Calibration of dolomite clumped isotope thermometry. *Chemical Geology*, *443*, 32–38. https://doi.org/10.1016/j.chemgeo.2016.09.021

Wright, D. T., & Wacey, D. (2005). Precipitation of dolomite using sulphate-reducing bacteria from the Coorong Region, South Australia: Significance and implications. *Sedimentology*, *52*(5), 987–1008. https://doi.org/10.1111/j.1365-3091.2005.00732.x

Zheng, W., Liu, D., Yang, S., Fan, Q., Papineau, D., Wang, H., et al. (2021). Transformation of protodolomite to dolomite proceeds under dry-heating conditions. *Earth and Planetary Science Letters*, *576*, 117249. https://doi.org/10.1016/j.epsl.2021.117249